CZECH TECHNICAL UNIVERSITY IN PRAGUE

Faculty of Electrical Engineering

Department of Electrical Power Engineering

Diploma Thesis

Study of Material Segregation in Mixed Halide Perovskite for Solar Cells

Author: Reema Pradeep Newaskar

Supervisor: doc. Mgr. Jakub Holovský, Ph.D.

Place: Prague, Czech Republic, 2021

MASTER'S THESIS ASSIGNMENT

I. Personal and study details

Student's name: **Newaskar Reema Pradeep** Personal ID number: **490232**

Faculty / Institute: **Faculty of Electrical Engineering**

Department / Institute: **Department of Electrical Power Engineering**

Study program: **Electrical Engineering, Power Engineering and Management**

Specialisation: **Electrical Power Engineering**

II. Master's thesis details

Master's thesis title in English:

Study of material segregation in mixed-halide perovskite for solar cells

Master's thesis title in Czech:

Studium segregace materiálu směsných halogenidových perovskitů pro solární články

Guidelines:

- literature survey
- mastering the I-V measurement in nitrogen atmosphere
- stability tests by illumination-relaxation cycling
- mastering the preparation of n-i-p architecture solar cells
- comparison of stability of materials with different Br-I ratio
- application of subbandgap absorption spectroscopy and photoluminescence

Bibliography / sources:

book: Kunwu Fu, Anita Wing Ho-Baillie, Kumar Mulmudi Hemant, Pham Thi Thu Trang,Perovskite Solar Cells: Technology and Practices, ISBN-13: 978-1771887281 ,ISBN-10: 1771887281article: J. Holovský, et al.,Lead Halide Residue as a Source of Light-Induced Reversible Defects in Hybrid Perovskite Layers and Solar Cells, ACS Energy Letters. 4 (2019) 3011–3017.https://doi.org/10.1021/acsenergylett.9b02080.article: S. Mahesh, et al.,Revealing the origin of voltage loss in mixed-halide perovskite solar cells, Energy & Environmental Science. 13 (2020) 258–267. https://doi.org/10.1039/C9EE02162K.

Name and workplace of master's thesis supervisor:

doc. Mgr. Jakub Holovský, Ph.D., Department of Electrotechnology, FEE

Name and workplace of second master's thesis supervisor or consultant:

Date of master's thesis assignment: **07.10.2020** Deadline for master's thesis submission: **21.05.2021**

Assignment valid until: **30.09.2022**

doc. Mgr. Jakub Holovský, Ph.D. Supervisor's signature	Head of department's signature	prof. Mgr. Petr Páta, Ph.D. Dean's signature

III. Assignment receipt

The student acknowledges that the master's thesis is an individual work. The student must produce her thesis without the assistance of others, with the exception of provided consultations. Within the master's thesis, the author must state the names of consultants and include a list of references.

Date of assignment receipt	Student's signature

Declaration:

I hereby declare that; I am responsible for the content of this thesis and the sources used for completing this study have been listed in the bibliography.

Date Signature

TABLE OF CONTENTS

LIST OF FIGURES

NOMENCLATURE

Isc	**Short Circuit Current**
Jsc	**Short circuit current density**
Voc	**Open circuit voltage**
FF	**Fill Factor**
SQ	**Shockley-Queisser**
Si	**Silicon**
CIGS	**Copper gallium indium selenide**
GaAs	**Gallium arsenide**
BaBr	**Barium bromide**
PV	**Photovoltaic**
PCE	**Power conversion efficiency**
OPV	**Organic photovoltaic**
QD	**Quantum Dot**
PSC	**Perovskite solar cell**
DSSC	**Dye sensitized solar cell**
HTL	**Hole Transport Layer**
HTM	**Hole Transport Material**
ETL	**Electron Transport layer**
ETM	**Electron Transport Material**
FTO	**Fluorine doped tin oxide**
ITO	**Indium doped tin oxide**
TCO	**Transparent conductive oxide**
MAI	**Methylammonium iodide**
CsI	**Caesium iodide**
FAI	**Formamidinium iodide**
PbI	**Lead Iodide**
Au	**Gold**
DMF	**Dimethylformamide**
DMSO	**Dimethyl sulfoxide**

I	**Iodide**
Br	**Bromide**
NiO	**Nickel Oxide**
TiO_2	**Titanium Oxide**
FTPS	**Fourier Transform Photocurrent spectroscopy**
FTIR	**Fourier Transform Infrared Spectrometer**
I-V	**Current-Voltage**
GHG	**Greenhouse gas**
CO_2	**Carbon dioxide**
PCBM	**Phenyl-C61-butyric acid methyl ester**
PTAA	**Poly (triaryl amine), Poly[bis(4-phenyl) (2,4,6- trimethylphenyl) amine]**
P_3HT	**Poly(3-hexylthiophene-2,5-diyl)**
PEDOT:PSS	**Poly(3,4-ethylenedioxythiophene) poly(styrenesulfonate)**
V_{I-}	**Iodide vacancy**
V_{Br-}	**Bromide vacancy**

ACKNOWLEDGEMENT

It feels a great sense of pleasure to have completed this research with great support and help from everyone involved directly and indirectly in this research. I would firstly like to thank God for showing me the right path, I would then like to thank myself for all the perseverance and dedication.

It would have been impossible to finish the research without the supervision, guidance and advice from Prof. Jakub Holovský. He genuinely helped me with allowing to perform the experiments safely at the University during the pandemic. So, I would like express my gratitude to him and Peter Amalraj Amalthas, Lucie Landova, Katarina Ridzonova and Lucie Abelova for their teachings and help during the experimentation. I would like to mention a thanks to the Institute of Physics, Prague for allowing me to do the necessary experiments for completion of my diploma thesis.

It goes without mentioning that the pandemic has been difficult for everyone and especially for students who are living abroad because the online learning can never replace the original form of teaching and learning, but I feel happy when I say that because of this thesis I was able to visit the laboratories in person and also work with people from different walks of life.

Lastly, I would like to thank my family and friends for providing the moral support and encouragement during the whole process.

ABSTRACT

Perovskite solar cell is an advanced and potential technology. It is a candidate for a top cell for potential tandem solar cell and with bottom cell as conventional crystalline silicon. The evidence of high efficiency of these devices has made researchers and scientist curious to study the technology more in detail.

The literature survey of this thesis sheds some light on the basics of solar cell technology. The thesis also gives briefs about few general terms used in photovoltaics. Moving further, the thesis goes into details about different types of solar cells. Since this study is focused on perovskite technology, the research done, focuses on perovskite technology in more detail.

This thesis includes the preparation and study of $Cs_{0.17}FA_{0.83}Pb(I_{0.6}Br_{0.4})_3$ perovskite solar cell. The study of phase segregation in mixed halide perovskite layers and solar cells has been completed using the optical and electrical measurements for observing the structural and electrical parameter changes. Finished cells and layers on glass were either prepared or supplied by partner laboratory. Defects occurring in the perovskites are also a part of this research. In this study, the phase segregation which accounts for one of the defects in the perovskite structure has been studied. To realize the segregation of the cell, time sequence of light soaking and relaxation in the dark and comprehensive analysis of the measured data was performed. From the obtained graphs it can be said that the reason for degradation might be due to ion migration when the cell is exposed to light soaking. It was also observed that during relaxation cycle, the perovskite cell structure returned to its initial state.

Additionally, this thesis includes the discussion of possible reasons for the degradation of sample due to illumination which comply

with the theory from various papers. This thesis also includes the study of stability and susceptibility to segregation for 5 different perovskite compositions. The Br-I ratios of the samples were different, which resulted in $FA_{0.83}Cs_{0.17}Pb(I_{0.68}Br_{0.32})_3$ being more stable than other samples.

CHAPTER 1

1. Introduction

1.1 Need for Renewable Energy Sources

The population on Earth is increasing at a rate of 1.75% per year [1]. With this increase comes the rise in the need of basic necessities for humans to survive. One of the basic necessities in today's world is Electricity. The current means of generating electricity is evidently harming the environment, humans and other life on Earth. Figure 1, depicts the effect of rise population over the years and their energy dependence. It is clear from the graph that there was a dramatic increase after 1950, due to massive burning of coal for electricity generation.

An interesting observation from the graph is, the rate of population increase is still lesser than other trends in the graph. This means the needs of each person is also increasing overtime. This trend is predicted to increase in coming years as well damaging the environment, unless there is way to find an efficient solution for this serious problem.

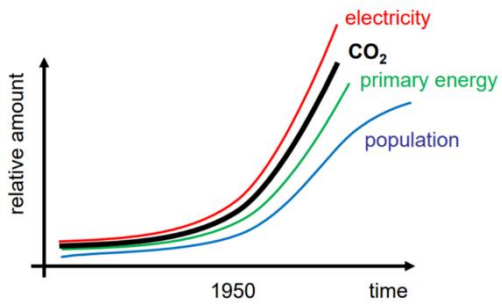

Figure 1 Relationship between rise in population and their energy needs [1]

To avoid the future problems, it is better to adopt means by which the environment remains clean and people healthy. "Renewable energy sources" is one of the many ways to make this happen. By using these sources, it can be possible to provide cleaner energy and reduce Green

House Gases (GHGs). Warming up of the Earth can be reduced to considerable extent if cleaner energy production is achieved. The effects of CO_2 on environment are huge and affect the atmosphere and human life is various ways causing sea acidification, melting of glaciers, rising sea levels, spreading of diseases and many more.[1]

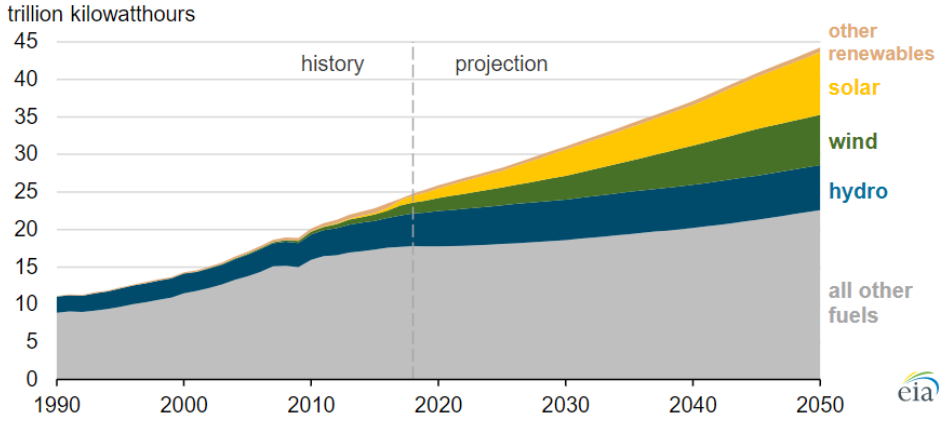

Figure 2 Renewable Energy Sources and its projection in the World [2]

Renewable energy sources will help in minimizing these effects and provide a better quality of life. The development of renewable energy sources was started a long time ago. Various research and development of available renewable sources have made it possible to get these technologies at current level. Figure 2, shows the development of different Renewable Energy Sources in the world throughout the years, it also includes projection of future years.

In Figure 2, it can be seen that energy from solar has high potential in the future years. The development in solar sector is tremendous in recent years and the technology has proven its efficiency as most of the countries in the World are not against solar. This technology of course requires future research and development, but it definitely shows the capacity to meet our needs.[2]

The sun is the primary and abundantly available source of energy. This readily available source is untamed and still far from being exploited. According to Elon Musk, "solar will be the single largest

source of electricity generation." The Sun is vital and essential for all the life forms on Earth, from photosynthesis to storing the generated

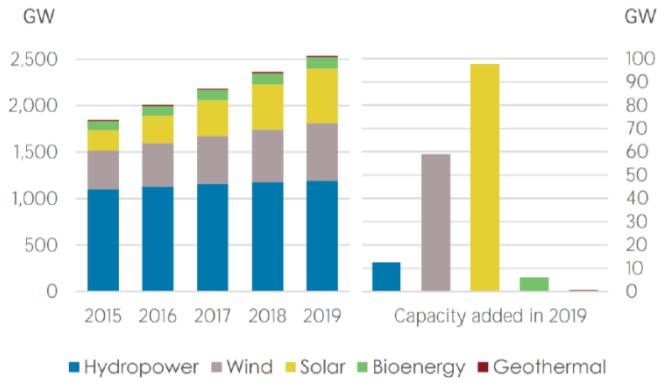

Figure 3 Renewable power capacity growth [1]

electricity, it has a huge potential for supporting clean human life. This resource is humongous with 5 billion years of hydrogen fuel available to burn in its lifetime.[3] This profusely available sustainable and clean energy will not be exhausted in near time, therefore, can be used to fulfil our electricity needs today. Additionally, solar energy offers benefits such as low emissions of Green House Gases (GHGs) or other gases harmful for the environment and life. Figure 3 shows the development in installation of solar energy. The graph shows increasing potential of renewable sources and also an increase in the installation of solar energy.[1]

To generate electricity, it is not enough to only make the light incident from the Sun on a glass. It has to be incident on a material which can conduct electricity. The most essential material required for power generation using the Sun is quartz or sand. This material too is plentifully available and most essential substance for mainstream silicon solar cell technology [4]. The chemical compound Silicon is a material obtained from sand. Up to 99.99% pure silicon can be obtained after the sand undergoes reduction reaction [5]. The thin-film technology has been studied a lot in the literature, crystalline silicon has attained the position of most successful solar cell material in the global PV market. In recent

years, perovskite solar cells have also gained technological attention due to its multiple light absorption ability, charge separation and transportation of electrons and holes in the materials [6].

CHAPTER 2

2. Literature Survey

A vast amount of information is available on the perovskite technology. The papers essential for this thesis are mentioned in this chapter, which are put together from the various works of researchers.

Fundamentals of solar cells and the technologies related to it form a foundation of studying in detail. Working of solar cell is a three-step process which includes, generation of electron-hole pair from absorption of photons, separation of pairs into charge carriers with the internal electric field and the extraction of carriers into external circuit. The solar cell technologies are First generation, second generation and third generation technologies. Third generation solar cell technologies include Dye Sensitized Solar Cell (DSSC), Quantum dot solar cell, Organic solar cell, Perovskite solar cell, Organic nano particle solar cell, Multi junction tandem solar cell technology. Focusing on perovskite solar cell technology, this technology is facing stability and device efficiency issues. It was able to obtain power conversion efficiency (PCE) of 12% for 10,000 hrs (around 1 year) which is much shorter than 25 years from commercialized PV technologies. The hybrid perovskite solar cell technology although has shown a rapid progress in terms of performance, is facing uncertainties with the mechanism between perovskite layer and other buffer layers [7]. Organometal halides perovskite solar cells are an emerging photovoltaic technology. In a liquid based dye-sensitized solar cell structure, the adsorption of methylammonium lead halide perovskite on a TiO2 surface produced a photocurrent with a power conversion efficiency (PCE) of around 3–4%, as first found in 2009. The PCE was doubled in 2 years by upgrading the perovskite covering conditions. These liquid based perovskite solar cells

have received little attention due to their stability issues. The instability in perovskite solar cell due to relatively high humidity was addressed by creating mixed halide perovskites. This was formed by mixing $CH_3NH_3PbI_3$ and $CH_3NH_3PbBr_3$, which resulted in having solid-solution of $CH_3NH_3PbI_{3-x}Br_x$ (x = 0–3). The property of bandgap tuning helped with stability in humidity soaking test. The inclusion of bromide in $CH_3NH_3PbI_3$ enhanced the stability of $CH_3NH_3^+$ cation in the lattice. A comparison of different perovskite structures attempted by different laboratories was made only to find out that as of 2014 PCE of 18% was achieved by the Korean Research Institute of Chemical Technology (KRICT), which was certified by the National Renewable Energy Laboratory (NREL). The inorganic materials in the cell are being replaced by organic molecular hole transporting materials (HTMs). $CH_3NH_3PbI_3$ and mixed halide perovskite $CH_3NH_3PbI_{3-x}Cl_x$ are at the focal point of investigation into high productivity perovskite solar cells. PCE of 29% is anticipated from tandem structures. Higher performance can still be achieved by making primary changes like thickness optimization of crystal, alongside band gap tuning. Modification of the bond distance and additionally point of X–Pb–X in $CH_3NH_3PbX_3$ is one of the ways to tune band gap energy. Lately, PCE moving toward 30% was accomplished from a single junction perovskite solar cell. The performance of perovskite solar cell depends on the excellent opto-electronic property of organometal halide perovskite material. Since PCE values over 20% are sensibly foreseen with the utilization of modest organometal halide perovskite materials, perovskite solar cells are a promising photovoltaic innovation. Under different conditions the parameters of solar cell can be measured. According to preferred experiments and test methods, the choice of measurement can be done to study the characteristics of solar cell [8]. Parameters such as open-circuit voltage V_{oc}, short-circuit current density J_{sc}, peak power P_{max}, fill

factor *FF* are used to calculate the power conversion efficiency of the solar cell. To attain optimum results, test under standard conditions should be performed. Using the empirical formulae, the performance of the cell under illumination and dark conditions can be studied. Solar cells are temperature dependent; their characteristics vary according to the temperature. From the electrical equivalent circuit of solar cell, the *J-V* characteristics and the resistance present in the circuit can be determined. The electrical equivalent circuit can be designed using single and two diode models, these designs can be used to determine the *J-V* characteristics [9].

Much of the research in photovoltaics is revolving around perovskite solar cells for better stability and improved efficiencies. The efficiency shown by these cells has progressed impressively, the best perovskite cells (efficiency under standard test conditions η= 25.2%) is competing with the silicon solar cell with efficiency η= 26.7%, despite the limited time since first experience with the research field. The theoretical thermodynamic limit known as Shockley−Queisser (SQ) limit for solar cells should be taken into account while designing and testing the solar cells. The reality that perovskite/Si tandems have as of late altogether exceeded the record for the Si single junction cell (η= 29.2% versus 26.7% respectively). Perovskite−perovskite and perovskite−CIGS tandems have efficiencies near the single-junction values, and further materials and gadget upgrades are expected to surpass these efficiencies. Maximum achievable efficiency limit according to the SQ limit is 32% [10].

A stable and highly efficient wide bandgap perovskite solar cell that promises high power conversion efficiencies are an important asset in multi-junction photovoltaic. Tuning the bandgap of the perovskite solar cells by changing the stoichiometric ratio of Br and I in organic-

inorganic mixed halide lead perovskite cells, improves the stability and PCE which is very important. To go around the instability issues of the perovskite solar cell, high Br content due to phase segregation and compositional engineering of A-cation site using methylammonium (MA), formamidinium (FA), cesium (Cs) or rubidium (Rb) was proven to be successful. The fabrication using spin coating method was used to prepare $Cs_{0.17}FA_{0.83}Pb(I_{0.6}Br_{0.4})_3$, on a double cation perovskite absorber layer. A bandgap of 1.72 eV was established during the measurements. Coating n-butylammonium bromide (BABr) on the double cation perovskite absorber layer, a 2D-Ruddlesden–Popper (RP) interlayer of intermediate phase is formed in between the absorber layer and the hole transport layer (HTL). The resulting cell exhibited an unprecedented 19.4% of PCE for wide-bandgap with Voc of 1.31 V, which was highest observed ratio of Voc over the maximum possible SQ limit, rising the expectations of others to achieve a higher PCE in the future [11].

Different types of coating are done while fabrication of perovskite solar cell. Chapter 1 from the Perovskite Solar Cells Technology and Practices describe in detail these coating processes. Various deposition methods are two-step deposition, single step deposition by spin coating, spray deposition. These methods are applied on different samples of solar cells and the parameters are tested for each sample to give a better understanding about the deposition methods [12]. Advanced characterization techniques of evading transient impacts in combination with solar cell performance have uncovered the subtleties of reversible light-illuminated perovskite degradation in vacuum. The study experiments revealed new information regarding the performance of the solar cell. According to the performed experiments reduced efficiency together with deep defects after minutes-long blue illumination, which vanishes after 1 hour in the dark were observed. The reason of this defect is also stated in the paper which was said to have occurred in the

fabrication process by the lead halide residual phase present in the material prepared by two-step method. This defect was confirmed using X-ray photoelectron spectroscopy. This defect is said to have solution, which is, preventing illumination of lead halide and single-step preparation of the cell [13].

The reason of voltage loss in the mixed halide perovskite cell is increase in Br content to widen the bandgap of the cell. The cell fails to perform optimally and fails to deliver the expected open-circuit voltage. This loss is related to the photo-induced halide segregation. A combination of Fourier Transform Photocurrent Spectroscopy FTPS along with detailed balance calculations are used to show the loss of Voc which result from halide segregation, thus giving a way to measure the effect of the low bandgap iodide-rich stages on execution of experiments. The authors state that, halide isolation isn't the prevailing Voc loss mechanism in Br-rich wide bandgap cells. But due to, moderately low initial radiative efficiency of the cells, which emerges from the two inadequacies inside the absorber layer and at the perovskite/charge extraction layer heterojunctions. The author thus suggests that focussing on maximising the initial radiative efficiency of the mixed halide films and devices is a higher priority than attempting to suppress halide segregation. The paper shows the value of Voc as 1.33 V which can be reached by a 1.77 eV perovskite bandgap even without suppressing halide segregation [14].

The fabrication method as mentioned in paper [15], has been used to fabricate solar cells for this thesis. Minute details mentioned in the manufacturing process helped greatly to fabricate the cells. The experimental method in the paper has been followed in detail with changes in perovskite layer deposition. Single step fabrication method is used in this thesis.

CHAPTER 3

3. Solar Cell Technology

3.1 Overview

Solar cell or photovoltaic (PV) cell is a technology that converts photons from sunlight to electricity. This process occurs due to the photoelectric effect. Photoelectric effect is a phenomenon used to generate electric voltage from the Sun's radiation. It is responsible for absorption of photons from the sunlight, energizing the electrons and generating the electricity which can be used in the appliances and equipment [16]. The solar cell is essentially made of n- and p-type semiconducting materials, responsible for generating electric voltage and electric current. These two semiconducting materials when joined together form a p-n junction. After joining of these two semiconductors electric field is formed at the junction region as electrons move to positive p-side and holes move to the negative n-side. The created field results in moving negatively charged particles in one direction and positively charged particles in other direction, thus producing electrical voltage [3].

PV energy is a renewable and can be used for almost all electricity applications, from urban to rural, centralized and decentralized power stations it has the potential to fulfil all the necessities [17]. This chapter includes a concise review of the basic solar cell technology, further text focuses on operation of solar cells and short summary of losses are presented.

3.2 Development of PV technology

The solar cell or PV cell can generate electricity directly from sunlight without any intermediate component. This conversion takes place with the help of photo-electric effect, explained earlier. A PV cell is

made using a semiconductor material called silicon, this material has the particular property of exhibiting photo-electric effect. The first modern-based PV cell was built by the scientists in 1954 at Bell Laboratories which had the efficiency of 6% [18]. This invention was a start of new era in PV industry, the development of first silicon solar cells to power space satellites, started by the early 1960s. The applications were very expensive and were not suitable for global use. During 1970s the real importance of solar cells was highlighted, this happened due to the first vast oil crisis. PV cells was considered as an alternative to the conventional power generation techniques. The development of cells began, resulting in quick increase in the conversion efficiency, shown in figure 4, the vast manufacturing globally significantly reduced the cell manufacturing costs.[3]

In late 1970s and 1980s, the first thin-film solar cells based on copper-sulphide/cadmium-sulphide junction showed the conversion efficiency of above 10% and these developed PV systems were focused on global applications. In the year 1975, the back-contact technology was

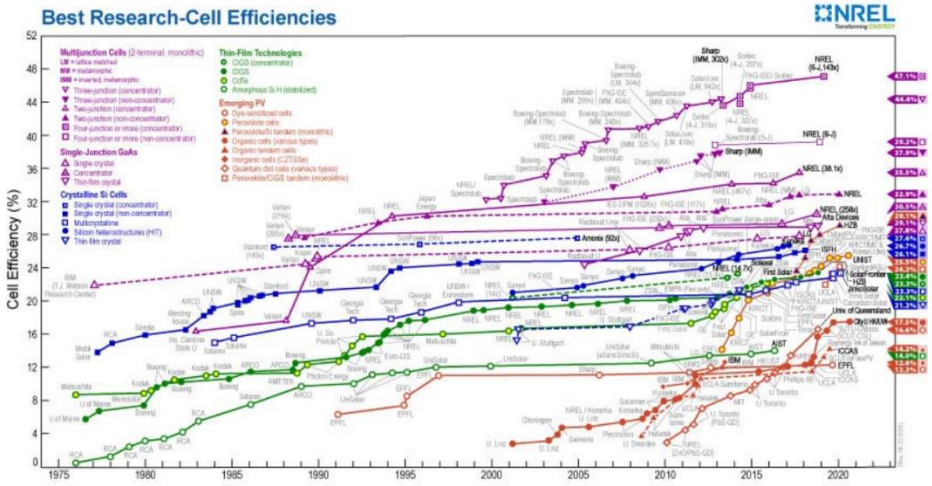

Figure 4 Development in the conversion efficiencies of solar cells [3]

introduced, featuring a front as well as rear contact. Different research around the world showed improved efficiencies, crystalline silicon (c-Si) reached the efficiency above 20% and in 1999 the efficiency reached

above 25%, considered as the highest in the world. National Renewable Energy Laboratory (NREL) built a solar cell based on gallium-arsenide tandem junction that exceeded the efficiency of 30%. Various laboratories world-wide continued developing the silicon PV cells, SunPower and Panasonic in 2014 reached new conversion efficiency records of 25%. Australian National University designed an IBC solar cell having rear contacts achieving 24.2% efficiency. Furthermore, by the end of 2016, Kaneka Corporation manufactured an IBC c-Si solar cell having the highest efficiency in the world of 26.33%. This back-contact technology has many advantages but has a complex configuration that requires specific configuration processes and has higher costs.[3]

3.3 Architecture of Solar Cells

3.3.1 Conventional Solar Cell

Conventional solar cell structure is based on simple semiconductor p-n junction diode operating under sunlight. When a photon is incident from the sunlight on the semiconductor material, a portion of photons is absorbed by the material, while remaining portion of light being reflected and transmitted through the semiconducting material. This results in formation of photon-generated electron-hole pairs. Due, to the built-in p-n junction the charge carriers are separated before they recombine and are collected at the cell terminals, resulting in flow of electric current in the external circuit. In this type of

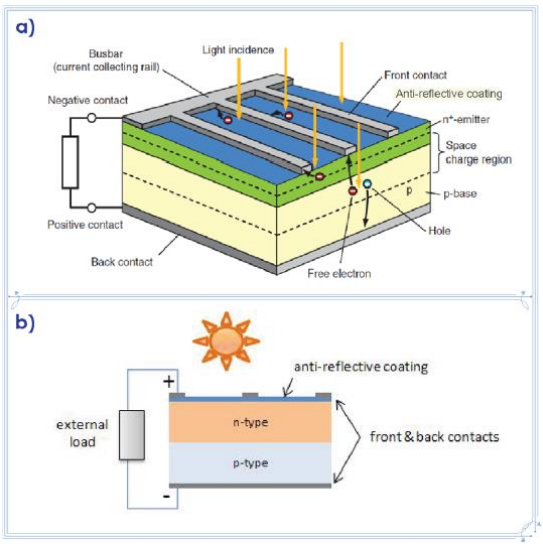

Figure 5 Conventional Solar Cell. a) 3-D view of conventional solar cell with front and back contacts, b) 2-D view of conventional solar cell [3]

technology, the main disadvantage was shading losses caused by the front contacts, shown in figure 5, on the surface of the cell. This prevented the sunlight to fully penetrate into the material. Transparency on the top surface of the cell determines the shading losses of the cell. The transparency in this technology is determined by the dimensions of the metal lines (front contacts) on the surface and distance between the metal lines[3].

3.3.2 Advanced Solar Cells

With research of previous years, the PV community has been continuously focusing on optimizing the design and performance of the solar cell, with main aim of achieving highest efficiency. All the research and development put together yields the best results shown by monocrystalline wafers. Silicon based cells showed the best efficiencies and can be classified into 3 main groups:

3.3.2.1 Passivated Emitter Rear Locally diffused (PERL) solar cell

Passivated Emitter Rear Locally diffused type of solar cell has two important features which minimises the recombination of electron-hole pair. One of the key features is, the top surface of the cell is surfaced with inverted-pyramid structure, also adding a double-layer anti-reflection coating to reduce the reflection from the surface and minimise the recombination of charge-carriers. The front contacts are made very thin using photolithography, to reduce the shading effect and losses due to it. These features help in reducing the optical losses resulting in higher current through the cell.

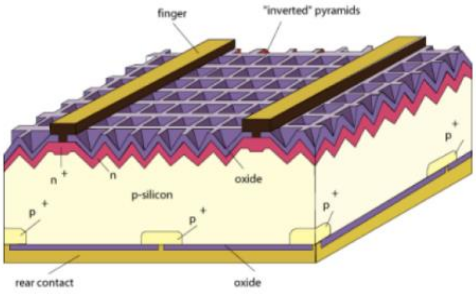

Figure 6 Structure of a high-efficiency PERL Solar Cell [3]

A selective emitter technique (heavily phosphorus diffused regions underneath the metal contacts) is applied at the rear side of the cell, while the top surface is lightly diffused. This can limit resistance at the contact and recombination at the rear while keeping good electrical contact. The efficiency recorded by these cells approaches 25% under the standard spectrum.

3.3.2.2 Silicon Heterojunction (SHJ) Solar Cell

The Silicon Heterojunction solar cell is a structure made out of two distinctive silicon-based semiconductor materials. One of these materials is applied as a thin layer between silicon and metal. This approach considers the laying down of a thin amorphous silicon (a- Si) layer, showing an evident rise of the open circuit voltage V_{OC}. Since a-Si has a

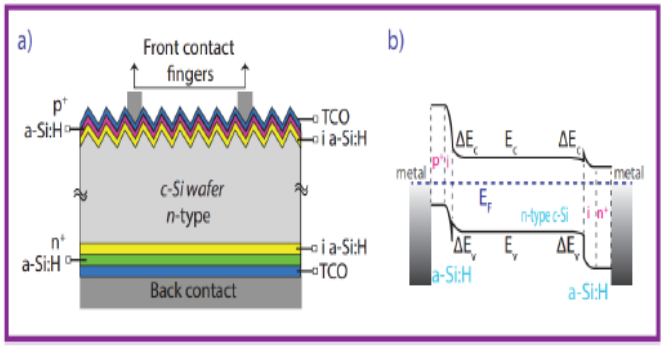

Figure 7 Schematic of SHJ. a) 2-D cross-section of silicon heterojunction cell, (b) Corresponding band diagram in dark at equilibrium [3]

wide band-gap layer, V_{OC} is improved and the high surface recombination in metal contacts is reduced. A schematic of a two-dimensional cross view and a band diagram of a typical silicon heterojunction (SHJ) solar cell are outlined in figure 6. The most recent record for the heterojunction silicon-based (c-Si) idea has revealed an open circuit voltage estimation of V_{OC} = 0.74V and an efficiency equivalent to 25.6%.

3.3.2.3 Interdigitated Back Contact (IBC) Solar Cell

The design has back contact where both the metal contacts are located at the bottom of the solar cell. Therefore, this is also called as back contact-back junction (BC-BJ) c-Si wafer solar cell. The conversion efficiency of these type solar cells is high, as there are no losses due to shadowing. Consequently, the carriers have to travel to the bottom of the cell to their respective collection centres, avoiding recombination. The BC-BJ solar cells are therefore very sensitive to recombination mechanism. The construction of an IBC solar cell is as shown in figure 8. The structure has alternating n-type and p-type layers on the bottom of the cell, they are represented by back surface contact (BSF) and emitter regions, respectively. These regions are responsible for collecting the charge carriers, the electrons are collected by BSF and the holes are collected by the emitter. The PV power is extracted from this cell, when the collected carriers flow through their corresponding metal point contact, placed just below the n-type and p-type region. [3]

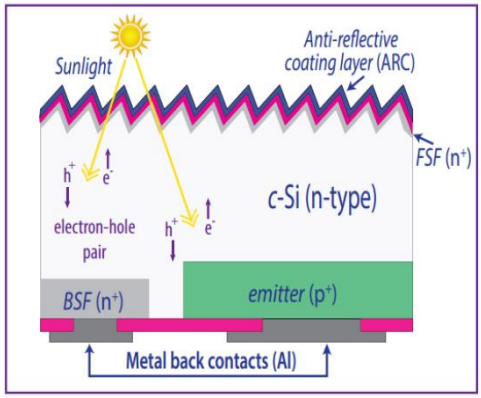

Figure 8 Schematic of simple single junction back-contact solar cell [3]

3.4 Operating Principle of Solar Cells

The working of a solar cell is dependent on the photoelectric effect, this effect was understood by Albert Einstein in 1905. During his work he realized that the incident light has a well-defined energy quantum, "photons". The energy of photons is given by:

$$E = h.v \text{ (eV)} \qquad (1)$$

where, h is the Planck's constant and v is the frequency of light. This explanation of Albert Einstein awarded him with the Nobel Prize in Physics in later years. The photovoltaic effect is closely associated with the photoelectric effect. Depending on the amount of energy the photon is able to transfer to the electron of the semiconducting material, the electron frees itself from the surface of the material. An ideal semiconducting material has 3 different *so called*, bands. The photoelectric effect depends on these bands and takes place in 3 processes [19]**.** These processes are studied at a very minuscule level and are as follows:

1. **Generation of charge carriers due to incident photons on the material**

Absorption of photons incident on the material are used to excite the electrons from its existing energy E_i to a higher energy level E_f, as shown in figure 9. If the energy of absorbed photon is high enough, an electron will be released from its *valence band.* Furthermore, the photon is absorbed only if the difference between the energy levels E_i and E_f of the present electron are equal to the energy level of photon, $hv = Ef - Ei$. In a good quality semiconducting material, electrons can be present in energy levels lower than *valence band*, E_v and higher than *conduction band*, E_c. Between these two bands is present a bandgap energy, $Eg = Ec - Ev$ where no electrons can be present. Photon with a lower energy if reaches the bandgap it will not be absorbed by the material and the photon will only pass through. [19]

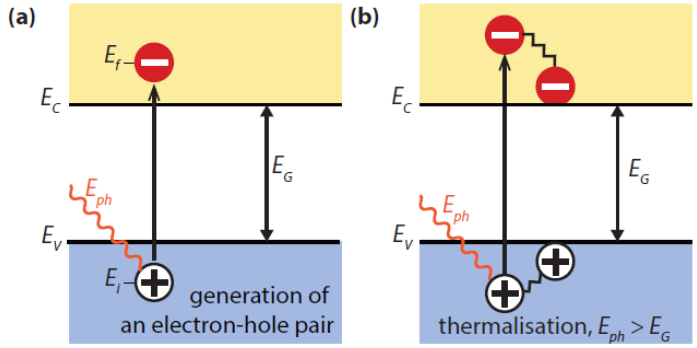

Figure 9 Illustration of internal process of solar cell a) illustrates excitation of electron due to photon absorption with bandgap, b) shows a part of thermalised energy when Eph > Eg [19]

When an electron is excited from *Ei* to *Ef*, a void is created at *Ei*. This void demonstrates behaviour of an elementary positively charged particle, "hole". Therefore, this absorption process leads to formation of electron-hole pairs, as shown in figure 10. The photon's radiative energy is converted to the electron-hole pair chemical energy. The maximal change effectiveness from radiative energy to compound energy is restricted by thermodynamics. This thermodynamic limit lies in the middle of 67% for non-concentrated sunlight and 86% for completely focused sunlight. [19]

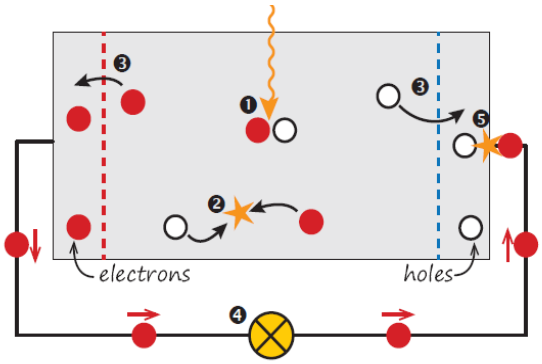

Figure 10 Example of simple solar cell working. 1) Photon absorption by the material and formation of electron-hole pair. 2) Electron-hole recombination under usual conditions. 3) Separation of electron-hole pair because to connection of semipermeable membrane. 4) Electrons pass through the connection to perform work in external circuit. 5) Recombination of electrons with the holes [19]

2. Separation of photon generated electron-hole pair at the junction

Generally, the electron-hole pair recombines, i.e., the electron falls back to its initial energy level. The energy absorbed by the electron is either released as radiative combination or is transferred to another electron or

hole. For extracting electrical energy from electron-hole pair the semiconducting material has to be connected with semipermeable membrane. This membrane is connected at both ends of the material such that electrons can flow out from one side and holes can flow out from the other side of the membrane, as shown in figure 10. Therefore, this function limits the solar cell in a way that the time required by the charge carriers to reach the membrane must be shorter than their lifetime, not allowing them to recombine. [19]

3. Collection of charge carriers at the terminal of the junction

The charge-carriers finally can be extracted from the solar cells to the external circuit to perform work through the electrical contacts. The chemical energy is converted into electrical energy. The electrons enter the electrical contacts, pass through it and recombine with the holes from other side of the contact, thus ready to drive the external circuit. This process is illustrated in figure 10 [19].

3.5 Bandgap of a solar cell

From the operating principle, it is clear that there is a lot of importance of the bandgap of the material used in solar cell. Losses in the cell technology are associated with the bandgap, therefore making bandgap a significant parameter in the construction of the cell. Bandgap refers to the energy difference between top of valence band and bottom of the conduction band. Electrons are able to jump from valence band to conduction band when some external force, such as photon from sunlight, is given to it. Electrons can gain energy either from external heat (phonon) or light (photon) to make the jump to the conduction band [20]. Only the photos with energy equal to

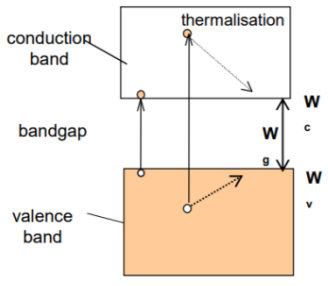

Figure 11 Typical depiction of bands in a semiconductor material [5]

the bandgap energy or higher than bandgap energy are responsible for creating charge carriers. Furthermore, the photons with lower energy than material's bandgap is wasted in the form of heat. Since not all photons have same energy, the photons with more energy than bandgap energy are considered as wasted surplus and these photons are re-emitted in the form of heat or light. This wastage of energy are losses which occur due to material's bandgap. The materials with larger bandgap can absorb more number of photons, whereas smaller bandgap material have different losses such as, thermal (heat) losses as mentioned earlier, consider figure 11 [5].

Bandgap energy changes with the material used for the PV cell. To consider an ideal solar cell, Crystalline silicon is the most popular solar cell semiconductor material. This material has a bandgap of 1.1 eV. To generate voltage using solar cell it is necessary to build a device with large bandgap. But on the other hand, it is necessary for the cell to absorb as much solar spectrum as possible which results in keeping the bandgap of absorbing material low. Therefore, bandgap between 1.0 and 1.7 eV makes the solar cell an optimum device (in this range, electrons can jump) without creating as much heat. Not all photons incident on the cell can generate electricity, the photon energy of light is different according to the wavelengths of light. The entire sunlight spectrum covers wavelengths in the range from 0.5 eV to 2.9 eV. This is the reason why semiconductors in solar cells do not respond to entire sunlight spectrum. Hence, solar cells are not 100% efficient [20].

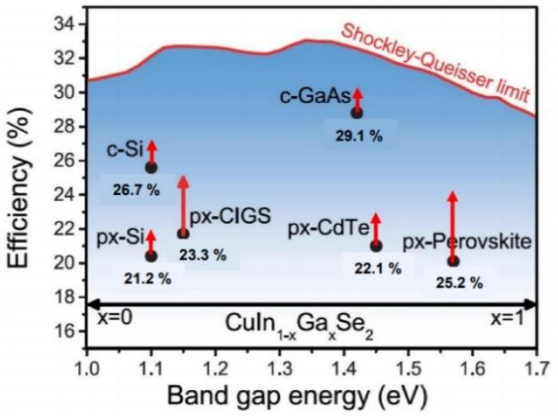

Figure 12 Theoretical Shockley-Queisser Limit [5]

As the losses are associated with bandgap of the material, the efficiency is therefore associated with the losses and hence with the bandgap. This relation between the efficiency and bandgap is shown in the figure 12 Theoretical Shockley-Queisser limit [21]. The graph shows maximum possible efficiency as a function of bandgap energy. This theoretical limit has two maxima as can be observed from the figure. The cell technology of c-Si and c-GaAs are comparatively better technologies in terms of efficiency. The Shockley-Queisser limit includes transmission, thermal and radiative recombination losses[21], [5].

CHAPTER 4

4. Third Generation Photovoltaics

Crystalline silicon based solar cell technology constitutes the first generation of photovoltaics. Amorphous silicon (a-Si), copper gallium indium selenide (CGIS), cadmium telluride (CdTe) forms the second generation in photovoltaics.

An emerging thin-film technology is being formed in the PV class, called as 3rd generation PVs. This generation has the potential to excel the current efficiency and performance. It includes organic photovoltaic (OPV), quantum dot (QD) and perovskite PV [22]. 3rd generation PVs focus on increasing the efficiencies, maintaining the economic and environmental costs. This technology aims to surpass the current theoretical efficiency limit by increasing the areal costs but hence reducing the cost per Watt peak. The fabrication of these solar cells is similar to second-generation thin-film deposition of solar cells but differ from that of the manufacturing of first-generation cells. Three PV generations are shown in figure 13, although the smaller area needed for a given power also decreases balance-of-systems costs, increasing efficiency strongly leverages lower costs, so that efficiency values well above 30% could significantly reduce these costs per watt [23]. To attain this efficiency improvement, devices aim to go around the Shockley-Queisser limit. The devices for this purpose have multiple energy threshold. Energy loss due to thermalization of photon energies exceeding the bandgap and inability of absorption of low energy level photons than bandgap are the disadvantages of single junction solar cell. This loss of energy accounts for about half of the energy of photons incident on the solar cells. Multiple threshold

approach can therefore be considered to utilize this otherwise lost energy.

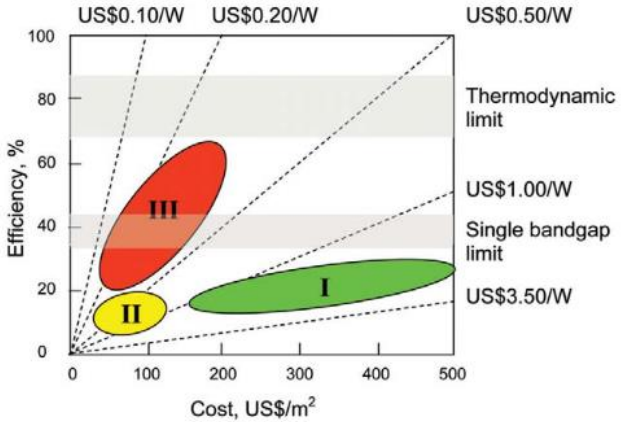

Figure 13 Efficiency and cost projections for first- (I), second- (II), and third-generation (III) PV technologies (wafer-based, thin films, and advanced thin films, respectively) [24]

4.1 Multi-level energy approach

This concept includes the use of multiple energy levels to absorb different sections of spectrum in various regions of the device structure [24].

4.1.1 Tandem Cells

The easiest configuration to understand and fabricate is the tandem cell configuration. It uses the concept of increasing the energy levels, solar cells with p-n junctions with different semiconductor materials and increasing bandgaps are placed on top of each other. The highest bandgap is on top therefore resulting the highest energy of photons from the Sun directly being absorbed in the top most layer of the cell.

Both photon selectivity and spectrum splitting are automatically attained in this stacking arrangement. A simplified schematic of a three-bandgap tandem solar cell is shown in figure 14. To draw an optimum power from the tandem cell choosing appropriate bandgaps, thicknesses, junction depths, and doping characteristics such that the solar spectrum is split between the cells is most important [24].

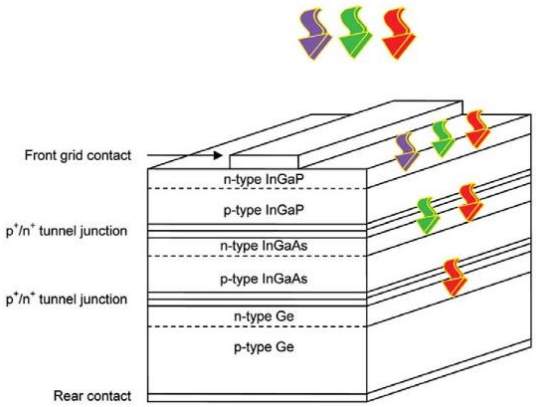

Figure 14 A simplified schematic of a three-bandgap tandem solar cell. The bandgap of each cell decreases from the front to the back, giving both spectrum splitting and photon selectivity [24]

CHAPTER 5

5. Perovskite Solar Cells

5.1 History of Perovskite Solar Cell

The history of metal halide perovskite solar cells goes back to the year 1839 when the crystal structure was named. The crystal was named after a Russian mineralogist L.A.Perovski. The crystal has a specific structure with formula ABX_3 [25]. The first organic-inorganic metal halide perovskites were reported in 1884 and 1892. Later in 1978 and 1995 methyl-ammonium lead halide ($CH_3NH_3Pbl_3$) and formamidinium lead halide ($CH(NH_2)_2PbI_3$) were reported, which are now commonly used as perovskite solar cells. Until year 2006, the properties of this material were focused on transistors and light-emitting diodes, in 2006 a conference presentation in Japan made a connection between perovskite and solar cells [26].

Organic metal halide perovskite solar cells have become prominent since their first evidence in energy conversion efficiency of 9.7% in 2012. Researchers around the globe have gained tremendous interest in the perovskite PV technology. High efficiency, ease of fabrication and cost-effective properties of these cells have resulted in rapid improvements in the technology, making it fastest developed solar cells with certified efficiency of 23.7% in year 2018 (refer figure 4) [26]. Strong optical absorption which can be compared with direct bandgap of semiconductors has made such rapid progress of this technology possible. Although the perovskite cells have lower carrier mobilities than Si and GaAs, they are still three or even more order of magnitude higher than many organic electronic materials. Longer carrier lifetime and sufficient carrier mobilities make organic metal halide perovskites a good choice for photovoltaics[26].

5.2 Structure of perovskite

To better understand the properties of perovskite material, it is important to understand the structure of perovskite. In this section, we will shed light on the structure of this mineral. Perovskite is calcium titanium oxide with formula $CaTiO_3$. The general formula of perovskite is ABX_3 , where A represents either inorganic or organic cation and B denotes divalent metal [27] with A being at the centre of the structure, larger than B, bound by X, an anion usually oxide or halogens [28]. All the materials with similar crystal structure as $CaTiO_3$, are termed as perovskites.

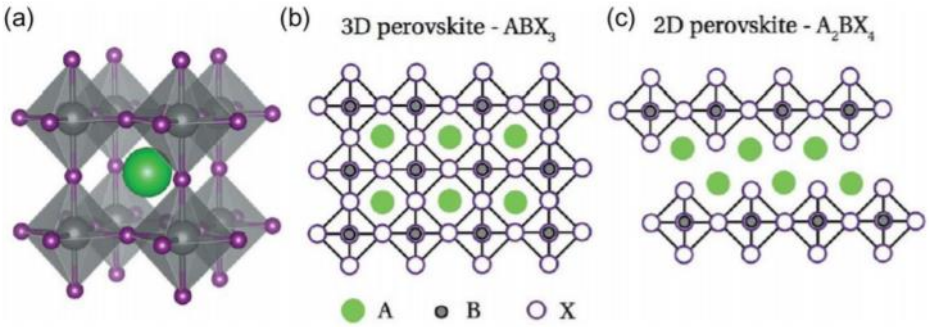

Figure 15 A typical perovskite ABX_3 crystal structure (a) The projected views of the three-dimensional ABX_3 perovskite is (b)while the 2-dimensional A_2BX_4 perovskite crystal structure is given in (c) [27]

In an ideal cubic perovskite, the relation between the radii of the two ions B-X and A-X is given by $R_A + R_X = \sqrt{2}(R_B + R_X)$. This relation was originally found only for structure ABO_3. In the year 1926, Goldschmidt defined a "*tolerance factor*", where he conveyed that the perovskite structure is still followed by ABX_3 compounds even though they do not exactly obey the relation between two radii, i.e.,

even if they are not ideal. The Goldschmidt tolerance factor plays an important role in the stability of perovskite and is given by:

$$t = \frac{R_A + R_X}{\sqrt{2}(R_B + R_X} \quad (2)$$

Where, t is the tolerance factor, R_A is the radius of A cation, R_B is the radius of B cation and R_X is the radius of anion. Stability and structural deformation of perovskite depend on the tolerance factor.

For ideal perovskite structure, the value of t is unity. The values having values less than unity ($\sim 0.75 < t \leq 1.0$) can also be termed as perovskite, such structures distort to a tetragonal or orthorhombic symmetry [29]. Figure above, shows the 3D structure of typical perovskite crystal. Different classes of perovskite such as organometal halide and alkali halide were studied widely. The ferroelectric and superconducting properties of oxide-based perovskites were extensively studied. The methylammonium lead halide $CH_3NH_3PbX_3$, is the most popular metal halide to be studied due to their improved optical and electrical properties [30]. The first breakthrough of methylammonium lead halide occurred with their use as light-absorbing material in a photovoltaic device. Perovskites are suitable for photovoltaic application due to their high absorption co-efficient, long diffusion length and superior charge transport properties to name a few.[28]

5.3 Device Architecture

The performance of a perovskite solar cell (PSC) is highly dependent on the device architecture [31] and the transport buffer layer present in the solar cell. Regular n-i-p structure and inverted p-i-n structure are the two fundamental structures to classify PSCs. These can further be classified as mesoscopic which incorporates

mesoporous layer and planer structure having all plane layers incorporated. The preparation of n-i-p or p-i-n configuration can be based on mesoporous scaffold titanium oxide (TiO2) or it can also be fabricated in simple planar configuration as shown in the figure 16 [27].

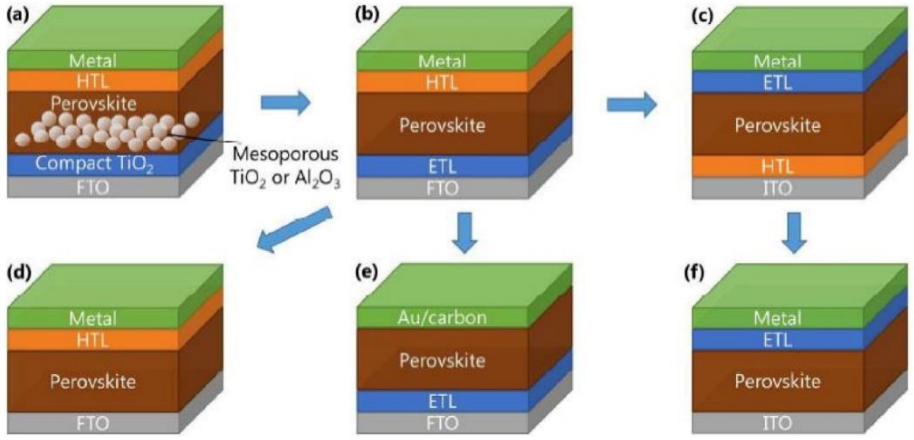

Figure 16 Various device architecture of perovskite solar cells (a) regular mesoscopic structure (b) regular planar structure (c) inverted planar structure (d) electron transport layer-free structure, and (e,f) hole transport layer-free structure [27]

5.4 Evolution of Device Architecture

In 2009, the architecture of PSC was based on liquid electrolyte in dye-sensitized solar cell (DSSC) configuration. This configuration was later discarded due to low performance factor, such as low efficiency (3.8%) and unstable nature of liquid electrolyte. This liquid electrolyte was then replaced by the first solid state hole transport layer (Spiro-OMeTAD) which improved the device performance significantly. Fundamentally, PSC structure is composed using 5 elements, a metal-based cathode, hole transport layer (HTL), absorber layer, electron transport layer (ETL) and transparent conductive oxide [32]. The transport layers decide the performance of the PSC. The HTL is responsible for collecting the holes from the absorber layer, transporting the holes to cathode and blocking the electrons. Having HTL with highest occupied molecular orbital slightly higher than the

perovskite absorber layer results proper functioning of the HTL. HTLs can be composed of various materials like Spiro-OmeTAD, NiO, CuO, CuI, Cu_2O, PTAA, etc. ETL has a function of collecting electrons from absorber layer and transport them to anode, blocking holes. Various ETMs used for constructing electron transport materials are TiO2, SnO2, SiO_2, ZnO, etc. Important performance parameters depend on the transport layers of PSCs. The transport layers should display properties such as good thermal stability, non-toxicity etc. Due to vast and evident work on the perovskite solar cells using different architectures the efficiency of solar cells improved up to 25.2%. [33]

5.4.1 Dye-Sensitized Perovskite Architecture

The first PSC developed in 2009 had dye sensitized structure, fabricated by Kojima and his colleagues. The fluorine-doped SnO_2 transparent conductive glass substrate was used. As hole blocking layer transparent conductive oxide (TCO), a counter electrode, a compact thin layer of TiO_2 (c- TiO_2 and thick mesoporous TiO_2 (m-TiO_2)) was used in the fabrication process, all the layers were sensitized over $CH_3NH_3PbI_3$ and $CH_3NH_3PbBr_3$ perovskite. The procedure used for fabrication was spin coating the precursor solution created by using equimolar concentration of methylammonium and lead halide. [33]

5.4.1.1 n-i-p structure of PSC

The fabrication of PSC using n-i-p structure is based on DSSC principle, where the perovskite absorber layer is self-assembled within porous region of TiO_2 layer. To protect the perovskite film and transfer electrons from conduction band of the cell a mesoporous layer of metal oxide is further deposited on the TiO_2 layer. This structure of device is popular for achieving high performance of the cell. Thin layer of TiO_2 as hole blocking layer forms the mesoporous layer, it is

deposited on conductive transparent oxide such as fluorine-doped tin oxide (FTO) or indium tin oxide (ITO). Penetration of perovskite precursor from the liquid form becomes easier due to thick porous layer of TiO_2 nanoparticles [27]

Planar configuration of n-i-p structure device are different, where the mesoporous layer is absent [27]. The structure of device comprised of TCO cathode, an n-type ETL, intrinsic perovskite layer, p-type HTL, and a metallic anode [33]. Perovskite film in this configuration is made thicker up to 300 nm and deposited on top of thick ETL, followed by deposition of hole transport material [27]. In 2013, Snaith et al. constructed dual-source co-evaporation of $PbCl_2$ and CH_3NH_3I and deposited the $CH_3NH_3PbI_{3-X}Cl_X$ layer over c-TiO_2 layer and attained PCE=15% [33] . Further continuing the structure of the device, to complete the device architecture metal anode is deposited [27].

5.4.1.2 p-i-n structure (inverted) of PSC

The position of ETM and HTM is reversed in this type of configuration, resulting the name inverted structure or p-i-n structure of perovskite solar cell. This configuration comprises of anode (TCO), a p-type HTL, perovskite intrinsic layer, an n-type ETL and a metal cathode. On ITO coated glass substrate, a 50-80 nm, p-type conductive polymer poly (3,4-ethylenedioxy thiophene) polystyrene sulfonate (PEDOT:PSS) HTL is deposited, this step is followed by deposition of up to 300-nm intrinsic perovskite thin-film. The last step to complete the architecture is deposition of (10–60) nm organic hole-blocking layer such as [6]-phenyl-C61-butyric acid methyl ester (PCBM) and a metal cathode (Al or Au). In inverted p-i-n configuration, ETMs can be selected from various options of organic to inorganic molecules. Recently, NiO and ZnO or TiO2 layers are being used for hole and electron selective contacts [27].

5.4.2 Buffer Layers in PSCs

Buffer layers in PSCs are used to improve the performance of perovskite devices [34]. When the free carriers are generated due to the photon-excited perovskite, the holes are collected by the anode and the electrons are collected by the cathode with the help of built-in electric field created by the asymmetric electrodes. The electrical contact at electrode/perovskite interface is critical to determine the device performance. The effective buffer layers must have energy level that align with energy level of perovskite. This results in minimizing the interfacial energy barriers at the corresponding interfaces and can help in achieving better charge collection efficiency and Voc of the device. Perovskite crystal growth can be affected by suitable energy from the bottom buffer layers. For example, charge recombination can be reduced by increasing the crystallinity of the device. This can be achieved by large-aspect-ratio of perovskite grains which can be found in hydrophobic HTL compared to hydrophilic HTL. To reduce the device Ohmic loss and maximize charge extraction, charge transport of p- and n-buffer layers needs to be appropriately high. According to Werner *et al*. if the conductivity of charge transport layer is higher than 10^{-3} S m^{-1}, the Ohmic losses are negligible.

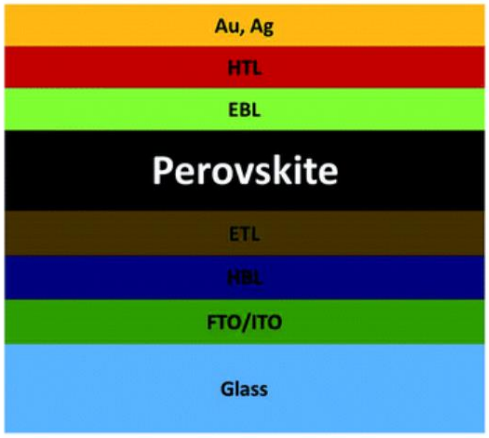

Figure 17 Schematic of Perovskite Solar Cell with buffer layers [7]

By using organic buffer layers high temperature sintering of TiO_2 [35] can be avoided, additionally providing other benefits like broad-spectrum of functioning tunability due to best chemical properties and good compatibility between flexible substrates [36] than inorganic material like TiO_2, SnOx, CuO, NiOx *etc*. for buffer

layers [35]. This flexible property of organic buffers has allowed researchers in innovating low cost and reduced dimensions portable devices. Moreover, organic buffer layers have characteristics like balance mobile ion between perovskite grain boundaries and provide barrier protection against moisture to halide perovskites to improve cell stability. [36]

5.4.3 Hole transport layer HTL in PSC

The materials used for HTL can be organic or inorganic. New HTMs are proved to improve the performance of the device. HTL is responsible for collecting and transporting free carriers to the electrode (anode) from the photo-active medium. General considerations for selecting the HTM are energy level alignment at interface for electron blocking and hole collection layer, high hole mobility, thermal stability and optical properties. [27]

5.4.3.1 Organic Hole Transporting Materials

These can be classified into sub-groups such as small-molecule p-type and conjugated polymers. Spiro-MeOTAD falls in the category of small-molecule p-type HTM and the examples of conjugated polymers can be given as poly(3-hexylthiophene) (P3HT), PCDTBT, PCPDTBT, and PTAA.

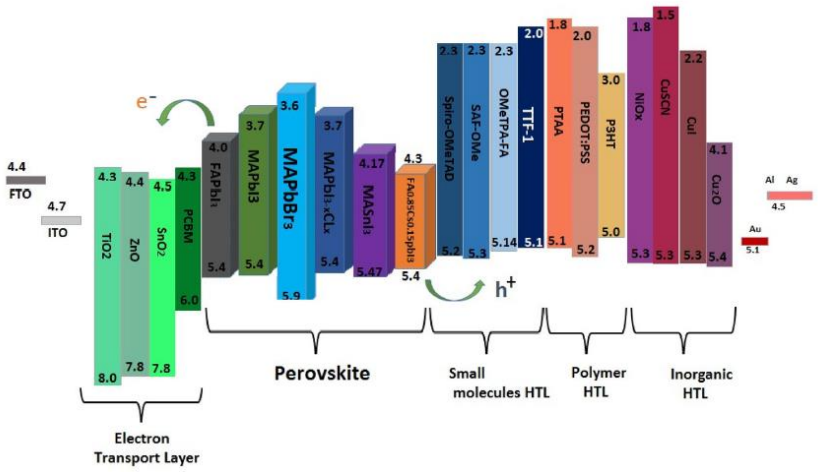

Figure 18 Schematic Diagram of energy level alignments of perovskite absorbers and common HTMs and ETMs with electrodes [27]

5.4.3.1.1 Spiro-MeOTAD

This is the most popular organic HTM used in PSCs. Spiro-MeOTAD has shown tremendous success in fabrication of high performing PSCs in short period of time. This was possible due to its property of ideal attraction for holes which can allows efficient collection and transportation of them from photo-active free charge medium to the respective electrode without recombination. The disadvantages of Spiro-MeOTAD is, its expensive and has restricted long term stability, low hole mobility and lower conductivity. This issue of Spiro-MeOTAD can be solved by adding necessary dopants to improve the electrical conductivity.

5.4.4 Electron Transport Layer (ETL) in PSCs

ETL is the layer in PSC where the electrons from the absorber layer are extracted and transported from the electron transporting material to the electrode. This layer is also called as electron extraction layer, the materials used for fabricating this layer range from metal oxides to metal oxide composites to metal oxide heterostructure nanoparticles [37]. The most important property for selecting the ETM is its alignment with perovskite layer and cathode [27]. Different types of metal oxides used as ETM can be TiO_2, ZnO, SnO_2, SiO_2, ZrO_2 these materials can help improve the PCE of the cell [37].

5.4.4.1 TiO_2

This material as ETM is the widely used and popular material for fabrication of PSCs [37]. Titanium oxide TiO_2, was firstly used in DSSC and later was used in porous state as electron transport layer in PSCs. TiO_2 has right band gap and also high transmittance which are the properties required in PSC for better PCE [27]. According to Snaith, TiO_2 based PSCs had lower stability than PSCs with absent layer of TiO_2. To solve this problem, solution was to use ultra-thin amorphous TiO_x instead of mesoporous TiO_2 for better electronic

stability. Other disadvantages of TiO_2 include high temperature annealing required by the material during fabrication process. Mesoporous TiO_2 used in PSCs have shown good efficiency, but on the other hand it suffers from hysteresis [37].

5.5 Types of Perovskite Solar Cells

5.5.1 Single-halide Perovskite Solar Cell

These cells were introduced as a new technology using single halide composite in photovoltaic technology. This new innovation gave a rapid boost in the research as they had never like before power conversion efficiency. An organic component methylammonium (MA) or formamidinium (FA) is a widely used perovskite absorber used in the single halide cells. Additionally, inorganic components are also used in the fabrication process. Most popular single halide solar absorbers are $MAPbI_3$, $MAPbBr_3$, $FAPbI_3$, $CsPbI_3$, and $RbPbI_3$.[27]

5.5.2 Mixed-halide Perovskite Solar Cell

Bandgap of absorber in the perovskite cell structure can be modified by using mixed-halide elements in the photoactive medium [27]. By manipulating the halide composition, the bandgap of mixed halide perovskite can be adjusted from 1.55 eV to 2.43 eV. Furthermore, when mixed halide perovskites are illuminated, halides possess ion migration property. This means that, when the sample is illuminated, bromide and iodide rich regions are formed which tend to reverse when kept in the dark [38]. $MAPbI_{3-x}Cl_x$ and $MAPbBr_{3-x}Cl_x$ are the most commonly used mixed halide solar cells since they revealed wideband optical absorptions and provided large carrier diffusion length. $MAPbI_2Cl$ was the first mixed-halide perovskite formed from precursor solution of N, N-dimethylformamide (DMF) comprising methylammonium halide and lead halide using spin-coating and reached PCE as high as 10.9% [39].

Mixed-halide perovskites such as $MAPbI_{3-x}Cl_x$ or $MAPbI_{3-x}Br_x$ are especially appealing because they exhibit superior photovoltaic efficiency such as limited exciton binding energy, higher electron mobility, and large lengths of exciton diffusion exceeding 1 μm. Various fabricating methods of preparing the mixed halide perovskite $MAPbI_{3-x}Cl_x$ utilised by researchers in world gave different resultant solar cell. Enhancing the light absorption by tuning bandgap using various concentrations of different halide species was observed during the experimentation. Using the precursor solution of halogens Cl and Br., Chiang et al. developed a high-quality mixed-halide $MAPb(I/Br/Cl)_3$ perovskite film via a one-step hot solution spin-coating technique. The investigation proposed that Br's presence could increase the V_{oc} values and boost the stability of the device[27].

CHAPTER 6

6. Perovskite Thin-film deposition Methods

Deposition of perovskite film on the substrate usually takes place using various deposition techniques. The deposition techniques involved in the fabrication process result in different morphology of the cell. These particular film structures determine the performance of the PSC. Widely used and low-cost methods of film deposition are one step deposition method and two step deposition method. One step and two step deposition methods also include spin coating method, which is also a very popular practice to coat the PSC [40].

6.1 Spin Coating Deposition method

The technique of spin coating method depends on centrifugal force principle. The substrates to be coated are placed at the centre of the spin coating equipment. The equipment rotates at the rpm (3000-4000 rpm) set by the user for particular amount of time (in sec). The solution by which the substrate is coated is prepared by dissolving in solvent. A drop of solution to be coated-prepared by dissolving in solvent acetonitrile -is deposited on the substrate placed horizontally at the centre of the equipment. Pipet is used to drop the solution on to the substrate. As a result, substrate is coated with a thin film of the solution.

Figure 19 Spin Coating equipment from Laboratory of Department of Advanced Photovoltaics, FEL, CVUT

6.2 One Step Deposition Method

Various techniques are involved in this deposition method by which perovskite film is deposited on the samples. These include solution processes such as spin coating, chemical vapor deposition, and dual source evaporation. One step deposition using spin coating has shown good results in the performance of the cell as shown in figure 20. In one step deposition method, all the precursors are mixed together in an organic solvent and then are deposited on the substrate. The film to be deposited is diluted with organic solvent dimethylformamide (DMF) and dimethyl sulfoxide (DMSO). Using spin coating method, the layer of the solution was deposited on substrate, spun at high speed to form a uniform layer on the sample. As a solvent chlorobenzene is added to improve the performance of the cell, it is spin coated on the substrate shortly after the first coat. The samples are placed for annealing on the hot plate at 100 ^{O}C for 30 minutes, where the samples are crystallized and change their colour to brown, refer figure 21.

Figure 20 One step deposition by Spin Coating in Nitrogen glovebox at FEL, CVUT

6.3 Two Step Deposition/Sequential Deposition Method

In this deposition method, PbI_2 is deposited first on the substrate and then it is transformed into perovskite phase. This method was first reported by Burschka et al., where PbI_2 was deposited on TiO_2 using spin coating method using an organic solvent. The formed films are annealed at 70 ^{O}C and then again spin-coated with methylammonium iodide CH_3NH_3I solution dissolved in

isopropanol. The samples are then transferred on the hot plate for 10 minutes at 100 ^{O}C, where they turn dark in colour. [26]

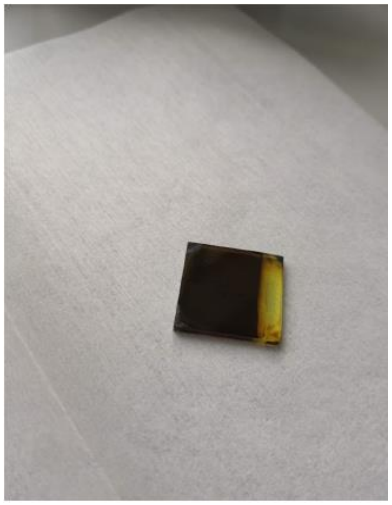

Figure 21 Resultant substrate after depositing chlorobenzene

CHAPTER 7

7. Challenges with Perovskite Solar cells

The perovskite solar cell technology faces many challenges when it comes to performance of the cell. Main issues consist of its performance in the environment where it is susceptible to oxygen and moisture. This leads to degradation of the cell resulting in the instability of the cell. According to the studies the PSC also shows photo-degradation, which accounts for a more serious challenge. The devices performance changes under different illumination and biasing conditions. They also show a feature of self-degradation in the dark in an inert nitrogen environment. This is caused due to the metal contacts corrosion present at the electrodes, which gives rise to ionic defects in the perovskite. Perovskite prepared from solution base have several defects mainly at crystal boundaries. Due to the presence of corrosive halide ions, contamination of the metal electrodes lead to performance degradation of perovskite solar cells [41].

With the development of efficient solar cells, fluctuation of device performance can be seen in the semiconductor devices. Due to various chemical interactions present in the semiconductor, possibility of defect formation has been observed and reported by many scientists. Formation of native defects in $MAPbI_3$ were mainly in the shallow electronic trap states i.e., the states lying close to the band-edges. However, with the help of experiments, the presence of deep trap states (within the perovskite band-gap) can be detected using various techniques which are Fourier transform photocurrent spectroscopy, photoluminescence quantum yield, X-ray diffraction etc. According to Shockley-Hall-Reed theory of recombination, thermal ionization levels placed deep in the band-gap have increased

trapping activity on charges which result in more prominent losses in the performance of the device. [42]

The defect formation in solution processed halide perovskite solar cell is unavoidable. Shallow form state of defects present close to the band edges result in doping the semiconductor in p-type or n-type and the deep state defects in the midlevel form recombination centres in the structure of the cell. So called "point defects" which greatly influence the performance of perovskites, are categorized in 3 ways 1) vacancy defects, 2) interstitial defects, where ions reside at the interstitial location of the lattice, 3) defects due to substitution of an atom with another atom. This one type of defect can also occur in pair with other type of defect called as Frenkel And Schottky defect. The Frenkel defect is due to combination of vacancy and interstitial defects and Schottky is a vacancy of anions and cations. Figure 22 depicts few of the possible defects present in the halide perovskite. Here the (ABX_3) perovskite lattice is represented by yellow, purple and blue dots respectively. [43]

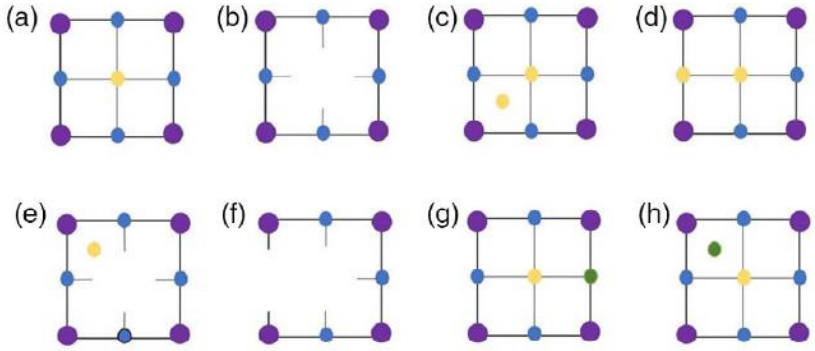

Figure 22 (ABX_3) perovskite lattice with possible defects present in the structure. a) perfect perovskite lattice, b) vacancy at site A, c) an interstitial defect, d) an antisite substitution, e) Frenkel defects, f) Schottky defects, g) substitutional impurity, h) interstitial impurity [43]

7.1 Phase Segregation of Mixed Halide PSC

As a developing technology, perovskite solar cell has defects. Perovskite material has excellent electronic properties as required for high efficiencies in photovoltaics. Bandgap of the solar cell, as

mentioned earlier, is an important factor which influences the electronic properties of the cell. The bandgap of perovskite solar cell can be easily tuned by altering the halide composition. The mixing of halide ions on x-site of the perovskite structure is an essential component to be considered and also brings out the versatility of the material.

Environmental effects such as continuous exposure to oxygen, humidity and illumination can cause instability in the PSC. Especially in the mixed halide PSCs, phase segregation is a particular type of instability which takes place causing instability of the material. This affects the electronic properties of the cell. In phase segregation, loss of phase stability and separation of halide ions of different type occurs due to exposure to above bandgap illumination. As a result, there are two different bandgaps (lower and higher bandgap) and varying halide composition formed in a good mixed halide PSC. Formation of non-homogeneous bandgap in the mixed halide perovskites limits the performance of the cells to a great extent [44]. According to a recent research, halide phase segregation includes effect of halide composition, segregated clusters formed at grain boundaries, formation/recovery kinetics and charge transfer. Many studies are concentrating on the reversible processes related to only the short-term light illumination of the device but ion migration during the long term illumination has its concerns on the stability and performance of the device [38].

To achieve highly efficient two terminal tandem solar cell, the choice of composite layers, to extract maximum energy from solar spectrum, is essential. Currently, lead bromide and iodide show a promising silicon/perovskite tandem solar cell. The bandgap of these components can therefore be adjusted through the ratio of two halide

ions. The results obtained from the Photoluminescence (PL) or Fourier-transform photocurrent spectroscopy FTPS techniques help in revealing the bandgap shift of the material under illumination. This bandgap shift is an undesirable characteristic in tandem solar cells and attribute to spatial segregation of the different halide ions of perovskite. In other words, the bandgap shift of the material separates iodide-rich region and bromide-rich region in the well mixed phase. This might be caused due to recombination, when illuminated the charge carriers form a channel and recombine in the new lowest-energy states (within the iodide rich phase) and creates the band shift of emitted light. Halide segregation also depends on the morphology of perovskite solar cell, with better quality of crystallinity the phase segregation is reduced. [45]

7.1.1 Ion Migration in Mixed Halide Perovskites

With a lot of research and experiments performed by many scientists all over the world, still there are many questions to be answered in regards with phase segregation of mixed halide PSC. Since, the halide segregation has already been reported, other aspects of the phenomenon still remain unanswered, which are most likely about the long-term irradiation of the perovskite crystal structure, effects of light-induced phase segregation on the performance parameters and most effective method to prevent this phenomenon. Instabilities due to illumination are responsible for optical and structural changes in the mixed halide perovskites. This leads to ion mobility in perovskite structure. Lead halide perovskites are well known for ion conductivity. From early literature, it was found that, the phase segregation is due to the existence of ion vacancies, interstitial sites and antisites in crystal lattice. Out of possibilities of various defects, halide vacancies of V_{I^-} and V_{Br^-} have the lowest energies. As a result, they are most common defects found in today's

mixed halide perovskite cell technology. The ionic conductivity measurements complying with theoretical studies stems from the vacancy migration activation energies (Ea values) for $APbI_3$ and $APbBr_3$. Consider the below table to refer the value of Ea which is sensitive to various factors related to ionic radius, ionic charge, crystal symmetry, migration distance and density of crystal defects.

Table 1 Activation Energy for Ion Vacancy Migration [46]

Vacancy	Ea (eV)
V_{Pb2+}	0.80-2.31
V_{MA+}	0.46-1.13
V_{FA+}	0.56-0.61
V_{CS+}	0.59-1.20
V_{Br-}	0.09-0.27
V_{I-}	0.08-0.53

From the above table it can be observed, the pattern of ion migration is from Br^- to Pb^{2+} going from most mobile ions to least mobile ions. The table shows, least amount of activation energy required for the ion to migrate in the perovskite structure. It can be therefore said that the most likely ion migration channels are related to halide vacancies V_{I-} and V_{Br-}. In addition, and to support the theory, recent studies have shown that halide vacancies play an important role in phase segregation of mixed halide perovskites. The phase segregation is observed to be reversible in the dark. It returns to its original state as it was in the fresh state when the behaviour of the cell is observed in dark [47]. Summing up, from [41], it can be said that the sizes of ions is an important factor contributing to ion migration. Smaller grain size not only is favourable for ion migration but it also generates ions.

7.2 Environmental Effects

According the study from [48], it can be understood that atmospheric effects have an impact on the perovskite crystal morphology. Conditions such as humidity, moisture and immersion of perovskite cell in different gases affect the halide segregation in mixed perovskite cells, resulting in degradation of this semiconductor device. There is enough evidence to prove the effect of atmosphere on the perovskite material, even though it is inconsistent but it can be observed through differences in material morphology, composition and experimental conditions. [44]

7.3 Hysteresis in PSC

Hysteresis is an anomaly caused in the behaviour of PSC, which can be due to the abnormal current-voltage characteristics, measured in reverse bias voltage. These characteristics depend on the scanning parameters such as scanning direction and rate of scanning. Hysteresis in light IV can be considered if voltage across the solar cell sweeps from low-bias to high-bias and immediately changes from high-bias to low-bias. During this process in the presence of hysteresis, the two IV curves do not super impose on each other. Hysteresis is also dependent on the size of grains in perovskite. Larger the grain size lower is the hysteresis in the cell, resulting in a stable performance of the cell [41]. Previous studies have hypothesized the origin on hysteresis could be i) defect density in perovskite layer, ii) interstitial ion migration, iii) formation of dipole polarization because of the ferroelectric properties of organo-metal trihalide perovskite. Hysteresis in perovskite is of two types normal and inverted hysteresis. While in both hysteresis the shape of J-V curve is have typical characteristics, in normal hysteresis, more photocurrent is extracted and in inverted hysteresis, the J-V curve has S-shape.

Instability in photoactive layer and low device performance are caused because of hysteresis in perovskite-based solar cell. [27]

7.4 Influence of defects on Solar Cell Performance

Although, mixed halide perovskite offers tuneable bandgap as a feature of tandem solar cells, an unfavourable phase segregation can take place when the cell is under illumination. There are serious effects observed on the optical and electrical response [43]. Point defects present in the device can adversely affect the performance of the cell. These defects can result into nonradiative recombination due to the deep level trap states for charge carriers. Surprisingly, these can form high-quality films but affect the performance in an unpleasant manner. The shallow defects present at the interface, edge or at grain boundaries of the cell may disappear due to the surface termination conditions, but it can limit the cell performance. The possibility of defect migration present at the interface between perovskite layer and carrier transport layer affect the efficiency of the cell. As mentioned earlier, this type of defect causes hysteresis in the I-V characteristic of the cell. The deep level trap states present in the halide perovskites or mixed halide perovskite is still a cause of great concern due to insufficient performance of the absorber materials of the solar cells [42].

CHAPTER 8

8. Fabrication of Perovskite Solar Cell

The experimental part of perovskite solar cell was done at the laboratory of CVUT, Faculty of Electrical, Department of Electrotechnology, Centre for Advanced Photovoltaics. The experimental part was completed in two tasks, first part being fabrication of the solar cell which lasted for three days and the second part was measurement of parameters of the solar cell taking another three days.

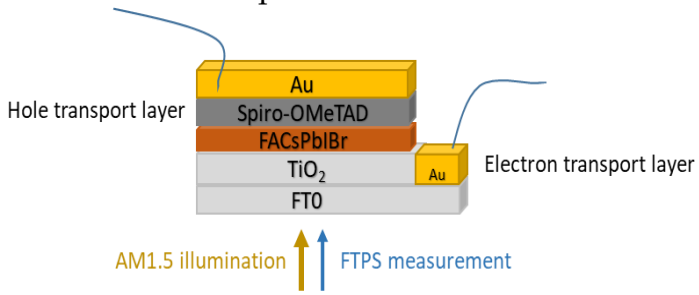

Figure 23 Perovskite solar cell structure used in practice

Fabrication Methodology

Cleaning and deposition of compact-TiO_2 (c-TiO_2) layer

Figure 24 fluorine doped tin oxide (FTO) coated glass substrates

Substrates were prepared using etched fluorine doped tin oxide (FTO) coated glass substrates. A total of seven samples were prepared for the experiment as shown in figure 24. The samples were cleaned by process of sonication using 2% Hellmanex detergent diluted in deionized water for 30 minutes as shown in figure 25 (left). The substrates were further cleaned by

sonicating using acetone and ethanol for 15 minutes each and were dried using nitrogen.


Figure 25 Cleaning by sonicating using acetone and ethanol (left). Spray pyrolysis for depositing TiO_2 layer (right).

For depositing the layer of compact TiO_2, spray pyrolysis was used as shown in Figure 25 (right) where the substrates were placed on a hot plate to dry as shown in figure 26. For c-TiO_2 layer, a solution was prepared by mixing titanium di-isopropoxide and anhydrous ethanol in a ratio of 1:9 using pipette. The hot plate was heated up to a temperature of 450 ^{O}C for 10 minutes and the clean substrates were then placed on the hot plate for 10 minutes. This helped in evenly spreading the layer of c-TiO_2 on the substrate while spray pyrolysis. After 10 minutes of heating the samples, they were sprayed with c-TiO_2 layer from a height of approximately 20 cm using the spray gun along with O_2 as the carrying gas. The substrates were sintered at 500 ^{O}C and allowed to cool down slowly at room temperature for 30 minutes.

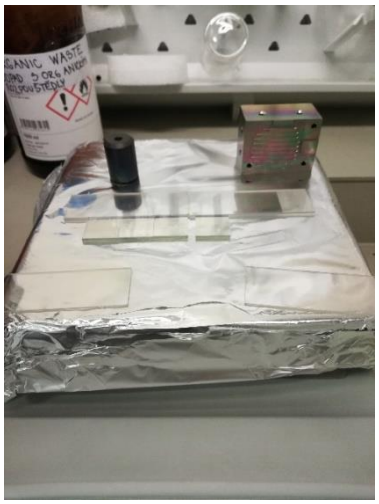

Figure 26 Substrates on hot plate to dry after deposition

Preparation of mesoporous TiO_2 (Electron Transport) layer

For deposition of next layer on the perovskite solar cell, 135 mg of titania paste was weighed on the balance and was mixed with 900 µL of anhydrous ethanol. The solution was sonicated for 10 minutes and then again for 20 minutes. The solution was prepared for next day use and again sonicated for 5 minutes. The deposition of m-TiO_2 layer was done using spin coating method on the substrates as shown in figure 28 (left). The seven substrates were coated with m-TiO_2 layer at 4000 rpm for 30 seconds each and were dried immediately on the hot plate for 10 minutes each. The samples were again sintered at 500 ^{O}C for 60 minutes. The m-TiO_2 layer was then doped with 20 mg Li-TFSI diluted in acetonitrile solution using spin coating at 3000 rpm for 30 seconds. The substrates after spin coating were sintered at 450 ^{O}C for 30 minutes and left to cool down again for 30 minutes as shown in figure 28 (right). The substrates were immediately transferred to the nitrogen glovebox (refer figure 30) for deposition of perovskite layer.

Figure 27 M-TiO_2 (Electron Transport layer solution)

Figure 28 Deposition of M-TiO2 using Spin Coating (left). Sintering of substrates at 450 ^{O}C for 30 minutes (right)

Preparation of Perovskite solution and layer

The perovskite solution was prepared by mixing different chemicals in specific amount namely CSI (88.34 mg), FAI (285.4 mg), PbBr2 (440.4 mg), PbI2 (368.1 mg) diluted with anhydrous

Figure 29 Magnetic stirring of perovskite solution (left). one step deposition of perovskite solution by spin coating (right)

dimethylformamide (DMF) and dimethyl sulfoxide (DMSO). The final compound from this mixture gives $Cs_{0.17}FA_{0.83}Pb(I_{0.6}Br_{0.4})_3$ solution to be deposited on the samples. Constant overnight magnetic stirring was done for mixing the solution at 60 ^{O}C as shown in figure 29 (right). The whole procedure was performed in the nitrogen filled glovebox. After overnight stirring, perovskite solution was filtered to remove the remnant undissolved particles to get pure perovskite solution. Deposition of the layer was done by one step method using spin coating, at 5000 rpm for 30 seconds. Chlorobenzene solution was again added on top of the perovskite layer after 30 seconds of spin coating of first layer again for 30 seconds (refer figure 29 left). The substrates changed their colour to brown and were dried on the hot plate for 30 minutes at 100 ^{O}C to crystallize the perovskite in the nitrogen filled glovebox.

Solution preparation for hole transporting layer

A hole transport layer was then deposited on the perovskite layer. For preparing the hole transporting layer, 75 µL of solution was prepared for deposition on the perovskite layer. Spirobifluorene was added in chlorobenzene with additional 28.8 µL of 4-tert-butylpyridine and 17.5 µL of Li-TFSI solution. The layer was spin coated on perovskite layered substrates at 4000 rpm for 30 seconds. The unfinished solar cells were stored in a dry box overnight, which helped in the oxidation process of spirobifluorene (hole transporting layer).

Figure 30 Nitrogen glovebox at CVUT FEL

Top Electrode of samples with Au

The seven perovskite unfinished cells were taken out of the dry box to evaporate Au back contact defined by shadow mask. To contact the underlaying FTO layer, the whole stack was scratched off on one

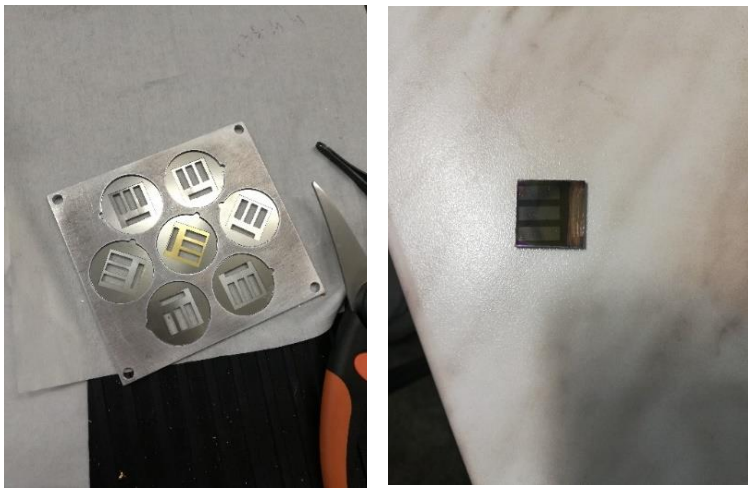

Figure 31 Shadow masking of solar cells with Au (left). Finished Perovskite Solar Cell (right).

side and the resistivity of that part was checked which should be around 20 Ω. This was done to complete a circuit of solar cell with this part being the lower electrode. Gold is a good conductor of electricity and is also suitable for these types of solar cells. Pure gold wire of 2.5 cm was melted and evaporated on the unfinished solar cells using thermal evaporator under high vacuum. Au pattern on the solar cell was done to mark the active area of the cell.

CHAPTER 9

9. Experimentation Methodology

9.1 Fourier Transform Photocurrent Spectroscopy (FTPS)

Fourier Transform Photocurrent Spectroscopy (FTPS) was used for the measurement of sub-bandgap absorption of the sample. An output light beam from Fourier Transform Infrared (FTIR) spectrometer is used to illuminate the device under test in this method. Using a calibrated photodetector, spectral dependence of incident light is measured. Hence converting the light irradiation into number of photons. The output light beam of FTIR spectrometer is an intensity modulated light beam. Signal collected from the investigated solar cell is demodulated by the internal electronics and control software of the FTIR. The extremely high sensitivity of this method can be useful in detection of sub-bandgap features of $Cs_{0.17}FA_{0.83}Pb(I_{0.6}Br_{0.4})_3$ perovskite solar cell. [49]

Sub-bandgap absorptance spectroscopy is a simple method to observe the defects in the device under test and is an acknowledged method in the field of photovoltaics. It can determine the semiconductor quality by examining the sub-bandgap absorptance and steepness of the absorption edge. Compared to the other methods available such as Photothermal Deflection Spectroscopy (PDS) which measures all the light converted to heat, while FTPS is sensitive only to light resulting to photocurrent. FTPS has the ability to measure the defect density in the absorber layer of a whole solar cell. [50]

9.2 I-V Measurements

I-V measurements are basic and an important means of measuring the parameters of the solar cell. These can be taken in light

(light I-V) and also in the dark (dark I-V). During this measurement, the voltage is applied across the cell to measure the current flowing through the cell. Power conversion efficiency can be determined from the light I-V curve. Recombination mechanism can be studied using the dark I-V curve. Dark I-V is measured in the dark or by obstructing the light path. Current can be then measured by applying the voltage across the cell [41].

9.3 Photo-induced Degradation

This measurement can be very useful in measuring the degradation of solar cell parameters (V_{OC}, I_{SC} and FF), when the cell is under illumination for several hours or days. It is a very important characterisation technique, when it comes to organic and perovskite solar cells as these devices show prominent changes in the performance when exposed to light. This measurement is carried out for a specific time interval usually under one sun illumination, the degradation of the cell parameters is observed in normalized scale.

Perovskite solar cells as mentioned earlier are vulnerable to the presence of oxygen and moisture. Therefore, to ensure the authenticity of this measurement, it can be carried out either in an Environmental chamber or a Glovebox. As both these apparatuses can be deprived of oxygen and moisture. Both the system can maintain an inert environment with pure nitrogen present in the systems [41].

9.4 Experimental Details

The FTPS and I-V measurements were performed in the laboratory of Institute of Physics, Prague. It took four days to complete the whole procedure of measurement, with remeasuring the samples which had few problems. The successfully measured samples were from Switzerland and the results are in the succeeding chapter. The

samples fabricated at the laboratory of FEL, CVUT were damaged during the measurement and therefore the results from those samples are not included in this thesis.

9.4.1 Experimental Setup

The perovskite solar cell was investigated by Fourier Transform Photocurrent Spectroscopy (FTPS) and I-V measurements. Thermo Nicolet 8700 FTIR device was used for measuring sub-bandgap absorption of the $FA_{0.83}Cs_{0.17}Pb(I_{0.6}Br_{0.4})_3$ perovskite solar cell as shown in figure 31. It was equipped with a tungsten lamp of 100 W, Stanford Research SR570 preamplifier was used to transform the photocurrent into electrical voltage. A set of colour glass filters was used to suppress the spectral regions with strong signal.

Figure 32 Thermo Nicolet 8700 FTIR (used for light modulation), Institute of Physics, Prague

The FTPS measurement was conducted along with 3 sun intensity light soaking at various time stamps from 0 minutes to 160 minutes, with intervals in between the corresponding measurements. Terminals to the PSC were switched from FTPS to I-V and extract the short circuit current (Jsc), open circuit voltage (Voc), fill factor (FF) of the cell. Labview software was used to perform the measurements. The samples were measured in nitrogen filled chamber with sapphire window. It was done to avoid the effects of air interfering with the procedure. The sample is specifically sensitive towards oxygen and moisture. The chamber was firstly removed of all the moisture by alternately filling with vacuum and nitrogen completing 3 cycles. The cell was light soaked for 3 suns

intensity of which it was later reduced to 1 sun for taking the I-V measurement. Devices were light-soaked at open-circuit, short-circuit and maximal power point (MPP) tracking regimes.

For the FTPS measurement, 3 different types of filters were used to measure the absorption of the cell as in figure 32 (right). Therefore, 3 different measurements were obtained under different conditions. The reason of using three different filters for this measurement is to

Figure 33 Front view of the measurement setup for FTPS and I-V measurement with 3 sun intensity light source Institute of Physics, Prague (left). Types of filters used for the experiment, Institute of Physics, Prague (right)

reduce the strong band-to-band absorption in order to observe the sub-bandgap absorption. FTPS measurement was conducted in the open circuit condition first. There was little to no change seen during the previous measurement of this cell performance, therefore changing the light soaking intensity to 3 suns was found to be an appropriate approach. The measurement was started initially with no filter and led to using combination of filters to study the absorption pattern of the PSCs.

Figure 34 Top view of the measurement setup for FTPS and I-V measurement, Institute of Physics, Prague (left). Side view of the measurement setup for FTPS and I-V measurement, Institute of Physics, Prague (right)

With alternately changing between the measurements, I-V curve of the cell was obtained. The measurements correspond to illumination of the solar cell for the above-mentioned intervals while measuring the different parameters of the cell. This method of measurement is called as illumination-relaxation method. Solar cell parameters like open-circuit voltage V_{OC}, short circuit current I_{SC} and fill factor *FF* were obtained during the period of measurement. The illumination cycle was followed by the relaxation cycle for similar time stamps.

"Open Circuit Voltage (V_{OC}) *of the cell can be defined as the maximum voltage available on the cell when current is zero. It is determined by setting net current value to zero in the solar cell equation:"* [51]

$$Voc = \frac{nkT}{q}\ln(\frac{Il}{Io} + 1) \qquad (3)$$

where,

Il - dark saturation current

Io - light saturation current

n – diode ideality factor

T – absolute temperature

k- Boltzmann constant

q- elementary charge

"***Short Circuit Current (I$_{SC}$)*** *can be defined as the current through the solar cell when the voltage on the cell is zero."*[52]

"***Fill factor (FF)*** *is a cell parameter which is related to the V_{OC} and I_{SC}, determines the maximum power from a solar cell. Fill factor can be defined as the ratio of maximum power from solar cell to the product of V_{OC} and I_{SC}. It is given by the equation:"*[53]

$$FF = \frac{Pmp}{Voc \times Isc} = \frac{Vmp \times Imp}{Voc \times Isc} \qquad (4)$$

where,

P_{mp} - maximum power from solar cell

V_{mp}- maximum voltage obtained from solar cell

I_{mp}- maximum current obtained from solar cell

Measurement continued the next day to measure other solar cell in short circuit condition. For the FTPS measurement, the cell was connected in short circuit. Light soaking was done again for the time stamps stated above. Light soaking was also performed in short circuit condition. I-V measurement was done similarly as the previous day using same time stamps, with only 1 sun intensity. After completing the measurement of FTPS and I-V in short circuit for 160 minutes under illumination, the cycle continued by relaxation in dark for another 160 minutes. During the measurement respective graphs of FTPS and I-V were observed to check for abnormalities/defects and phase segregation of iodine and bromine, which affect the performance of the perovskite solar cell.

The graphs were obtained after calculations and normalization of the measured data. From the graphs, sub-bandgap absorption of the

sample can be seen from the 0.8 eV – 1.5 eV. The graphs obtained are plotted for the time stamps of sample illumination and relaxation cycle in the logarithmic scale, so that small changes in the sample can be observed clearly. It can be observed that, the sub-bandgap absorption in the sub-bandgap region is increasing throughout the time. This can happen due to the deep defects present in the sub-bandgap regions. In the open circuit 3 suns illumination cycle graph, the deep level defects in the sub-bandgap absorption region are increasing. From 1.5 eV – 1.8 eV, phase segregation takes place, the exact reason for this happening is still unknown however, according to literature present in [42], [43] it can be said these are because of the deep level defects explained earlier. From the relaxation cycle graph, it can be observed that the phase segregation relaxes, i.e., the segregation of iodide and bromide regions in the cells go back to their initial state. Connecting the terminals of solar cell in short circuit for obtaining the measurements, graphs 3 and 4 were observed with 3 suns illumination. In the illumination cycle, it is seen that for 5, 10, 20 minutes the sub-bandgap region from 0.8-1.5 eV is increasing, but the changes are very small between the time stamps. After the 20 minutes light soaking, there is a drastic increase in the sub-bandgap absorption. This is due to the deep defects present in the perovskite cell. The explanation for the other regions of these graphs is similar to those of open circuit measurements. The graphs show a lot of prominent changes in the samples under illumination and relaxation cycle. Where the sub-bandgap absorption can be seen increasing during the illumination cycle due to the present deep defects, the phase segregation can be also observed in the higher energy level. As suggested in many papers, the sample was behaving in the similar way during the light soaking and relaxation period.

CHAPTER 10

10 Results and Discussion

The samples prepared at the laboratory of FEL, CVUT did not yield good results and the results were not included this work. Therefore, we used samples provided by EPFL PV-lab in Switzerland of the similar composition and went ahead with performing the experiments on them.

We performed the experiments using two intensities of light. Few measurements were completed using 1 sun intensity and later

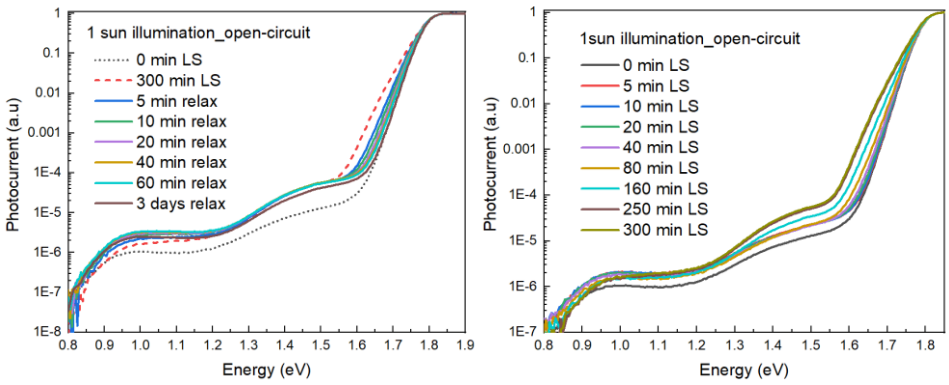

Figure 35 Illumination cycle under 1 sun intensity (left). Relaxation cycle under 1 sun intensity (right).

continued to 3 suns intensity on different set of samples. The evaluations and graph plotting were performed using the Origin Software. The graphs are obtained by plotting photon energy (eV) of the measurement probe beam on the x-axis and the corresponding photocurrent produced due to the illumination on the y-axis.

There can be seen considerable difference in the 1 sun intensity and 3 suns intensity graphs. The results from 1 sun intensity figure 34, were not very prominent in showing significant changes in the sub-bandgap region absorption. It showed very small changes in the sub-bandgap region where the phase segregation was taking place.

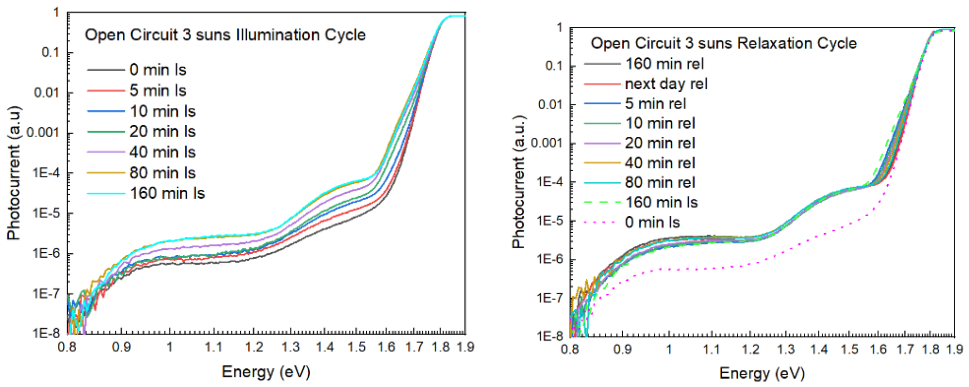

Figure 37 (Open-circuit) Illumination cycle under 3 suns intensity with increasing phase segregation (left). Relaxation cycle under 3 suns intensity with decreasing phase segregation (right).

Compared to the other graphs-with the 3 suns (figure 36 and 37)-the phase segregation in the 1 sun graphs is not observed. During the 1 sun illumination we were able to observe changes at the absorption edge but there were very little to no changes observed at the sub-bandgap region because of phase segregation. Therefore, we decided

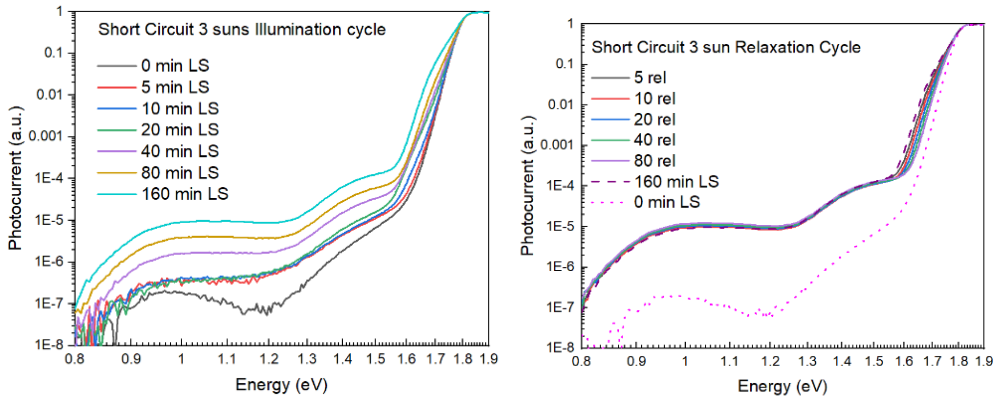

Figure 36 (Short Circuit) Illumination cycle under 3 suns intensity with increasing phase segregation (left). Relaxation cycle under 3 suns intensity with decreasing phase segregation

to increase the intensity to 3 suns to observe more significant changes happening due to phase segregation at the sub-bandgap region. The

phase segregation observed at sub-bandgap absorption, in the figure 43-46 are present but still do not show much drastic changes in their pattern. In other words, it can be said that, the samples from Switzerland showed the changes in the properties and performance which complied with the theory, but the changes were not drastic even after increasing the illumination intensity. We hoped to see more prominent phase segregation. According to our theory, the stability seen in the Swiss samples may be because of enlarged grain sizes, as mentioned earlier and in the studies [54],[55],[56], larger grain sizes result in reduced phase segregation.

10.1 Mechanism during Illumination and Relaxation

Here we focus on the fundamental mechanism of Illumination Relaxation cycle. During the illumination of sample and the property of mixed halide perovskite, iodine interstitials I_i^+ are created as according to [57], [58], [59] iodine is less bounded in the lattice than bromine. These ions tend to move towards the grain boundaries where they are more energetically stable. Therefore, resulting in a positive space charge at the boundaries and negative space charge at the grain interior created due to iodine vacancies V_I^-. The presence of positive space charge has been confirmed by many studies at the grain boundaries which can support our claim that it can be due to the accumulation of I_i^+ defects at the grain boundaries. Furthermore, this results in forming an I-rich layer of thickness of few nm during the light-soaking (LS). The unnecessary I_i^+ then slowly combine with the lattice of maternal mixed halide perovskite and begin to form iodine-

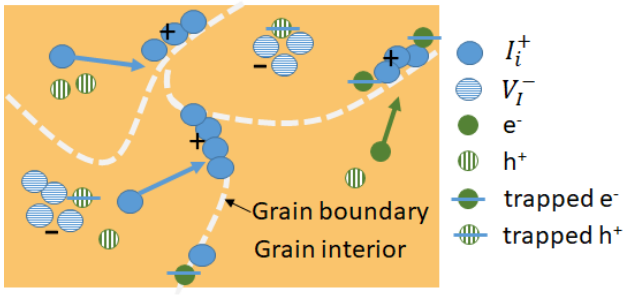

Figure 38 Illustration of illumination and relaxation mechanism

enriched polycrystals in the vicinity of the grain boundaries giving rise to phase segregation. Studies have also shown that the phase segregation takes place at the grain boundaries rather than at the grain interior and that the iodine rich domains are preferably present at the grain boundaries.

During light soaking, the holes are created due to illumination and are trapped at the V_I^- defects at the grain interior. The electrons generated due to illumination are trapped at the grain boundaries due to I_i^+ defects. This results in compensation of positive space charge at the grain boundary. This phenomenon is more prominent in the open-circuit condition of the sample due to high concentration of photo-generated carriers. On the other hand, in the short circuit condition, the space charge due to the halide defects are maximized because of low concentration of charge carriers available to compensate them.

Focusing on the fundamental regime of relaxation cycle, we observe reversibility of phase segregation. During relaxation of the sample, no free excess charge carriers are available. As a result, charged defects and the dipole between the positively charged grain boundaries and negatively charged grain interiors takes place as trapped carriers recombine within few ns. The positively charge iodine interstitials are drifted back to grain interior due to restored electric filed. This exchange mechanism at nodal positions causes intermixing in the device. This behaviour explains reversibility of phase segregation. Reversibility is hence an important factor to not only understand relaxation of mixed halide perovskite but also to understand stability of the mixed halide perovskites due to phase segregation.

I-V measurement results

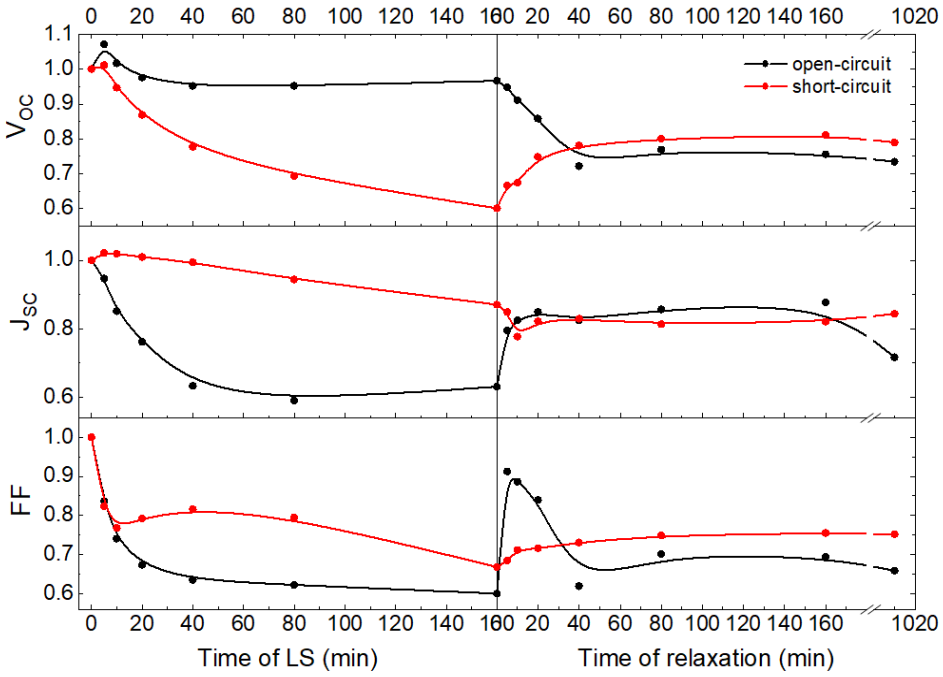

Figure 39 Evolution of Voc, Isc and FF vs time curves. Parameters of solar cell during the time of illumination and relaxation cycle during measurement.

Figure 39 shows the behaviour of solar cell parameters during the entire time span of the measurement. The parameters are defined in the previous chapter and tell us about the performance of the cell throughout the changes happening in the sample. It can be observed from the graph that, the parameters are not constant and have drops and peaks, showing the instability of the sample. This can be the result of defects in the sample and as mentioned in the paper [60], suggests this can be caused due to the hysteresis effect in the cell. The paper also suggests a possible link between halide separation and the J-V characteristics of mixed halide perovskite solar cell. This mainly affects the electrical parameters of the cell, hence resulting in lower efficiency. The graphs observe a decreasing trend during the light soaking as the duration of illumination increases and interestingly, in the relaxation cycle, the sample tries to almost recover and reach its initial state. According to [14], the loss in Voc is associated not only to

halide segregation but also depends on other factors showing more prominent loss in V_{OC} such as non-radiative recombination losses.

Photoinduced phase segregation is therefore one of the peculiar characteristics of this hybrid material caused due to its electrochemical properties. The iodide-rich and bromide rich regions formed during the illumination hinder the practicability of this device. As mentioned in [38], the clusters enriched in one of the halides formed at the grain boundaries are responsible for the fluctuations and instability of the device. The paper also researches if the phase segregation is taking place due to scanning electron microscopy (SEM) and finds out that, during SEM the phase segregation cannot happen due to the electron beam itself. It mentions about molecular simulation suggestions, being, the phase segregation might be a result of charged excitations producing enough strain on the lattice to destabilize the solid solution, supporting the separation of halides. Various theories proposed in the [61], [38], [60], [62] for the formation and the reasons behind it make it difficult to pin point single reason for this disturbance in the sample, but interestingly the pattern of formation of halide segregation using various halide compositions or different materials at A site of the perovskite, show similar behaviour when illuminated in light and relaxed in the dark.

From the discussions and the obtained results, it can be said that, the J-V and FTPS measurements are complying with the above discussed illumination and relaxation cycle mechanisms. An interesting study which came along with this research are the causes of stability in the Swiss samples stating the fundamental and exact knowledge of reversibility can be used for suppressing the phase segregation, by promoting relaxation mechanism, by improving the

charge collection efficiency of the devices and thus preventing the compensation of dipole between grain boundaries and grain interior.

CHAPTER 11

11 Effect of various I-Br compositions on Phase Segregation

11.1 Preparation of mixed halide perovskite

This additional research includes study of phase segregation of mixed halide perovskite thin films using different compositions of PbI_2 and $PbBr_2$. Here, 5 different samples were prepared in the Centre for Advanced Photovoltaics at FEL, CVUT. Glass substrates were cut into 20x20 mm pieces. Glass substrates were cleaned in an ultrasonic bath at first in acetone for 15 minutes, thereafter in isopropyl alcohol for 15 minutes, finally in deionized water for 15 minutes. All substrates were dried by blowing nitrogen. All the samples were prepared in 2 days and then measurements were continued on them. Solution preparation and perovskite layer deposition was done in the glovebox in a nitrogen atmosphere. All samples were stored in glovebox covered by Al-foil protected the samples against the light. Samples were prepared using different ratios of PbI_2 and $PbBr_2$. The compositions used are as $FA_{0.83}Cs_{0.17}Pb(I_{0.76}Br_{0.24})_3$, $FA_{0.83}Cs_{0.17}Pb(I_{0.68}Br_{0.32})_3$ $FA_{0.83}Cs_{0.17}Pb(I_{0.6}Br_{0.40})_3$, $FA_{0.83}Cs_{0.17}Pb(I_{0.52}Br_{0.48})_3$, $FA_{0.83}Cs_{0.17}Pb(I_{0.44}Br_{0.56})_3$. As mentioned in the fabrication chapter, these samples were prepared in the similar way. The perovskite layers were spin coated on the glass substrates along with chlorobenzene, which gave the transparent glass substrate its brown colour. The substrates were spun at 1000/5000 rpm with 100 µl of solution for 1st and 2nd step respectively. At 100 ˚C the samples were sintered on hot plate for 30 minutes. The purpose of this measurement was to observe the changing patterns of absorptance with different mixed halide compositions

11.2 Optical Characterization and Experimental Setup

For measuring, the samples were cut in 1x1 cm squares so fit into the testing equipment. I performed an analysis of spectral dependence of light reflected and transmitted by FACsPbIBr samples. I measured the reflectance (R) and transmittance (T) using Integrating Sphere. Using these measurements, the absorptance (A) of the incident light absorbed was calculated by using the formula:

$$A = 1 - R - T \qquad (5)$$

This study is focused to observe the rate of phase segregation of different compositions of mixed halide perovskites. The behaviour of the samples under different conditions changes. I performed the experiments using the time stamps of 10 minutes, 40 minutes and 80 minutes of light soaking with Xenon Lamp on all the prepared mixed halide perovskite layers. This regime was chosen to ensure and record the changes happening at the start, middle and end of the experiment. Light soaking was done in the cryostat filled with nitrogen with illumination of 1 sun (determined by calibrated photodiode)

11.3 Results and Discussion

Here I have obtained the results from measuring the five samples using integrating sphere. These results are evaluated using Microsoft Excel keeping absorptance and wavelength (nm) on y and x-axis respectively.

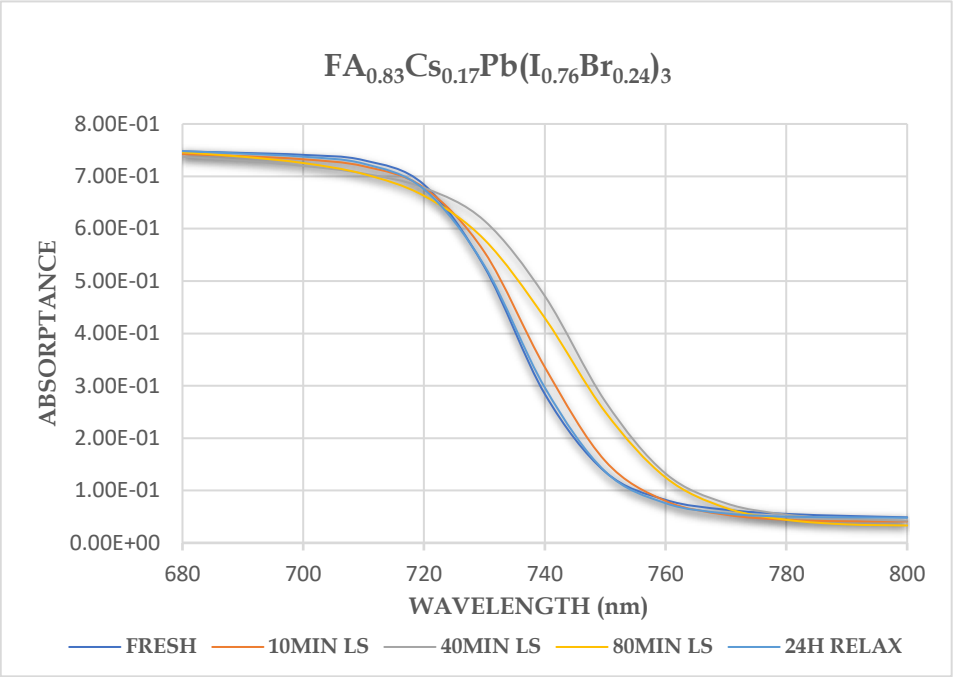

Figure 40 Calculated Spectral dependence of absorptance of perovskite on glass for composition $FA_{0.83}Cs_{0.17}Pb(I_{0.76}Br_{0.24})_3$

Interesting results can be observed from all the graphs with different composition of perovskite solution. This can pave a way in helping us decide about the optimum way of fabrication and determine better optical properties of the samples. All the samples used showed different results in absorptance. The sharp absorption edge is seen occurring at different wavelengths in all the samples. Figure 40 with composition $FA_{0.83}Cs_{0.17}Pb(I_{0.76}Br_{0.24})_3$ can be observed in the graph, where a sharp absorption edge is seen at λ= 720 nm. The absorption edge is seemed to shift from λ= 720 nm to λ= 730 nm after 40 minutes of light soaking. After relaxation of sample in dark, the absorption edge is reduced to its initial wavelength of λ= 720 nm. In most of the samples one thing can be commonly observed is, after relaxation of samples in dark, the shift of absorption edge is reduced compared to the absorption edge of 80 minutes light soaking.

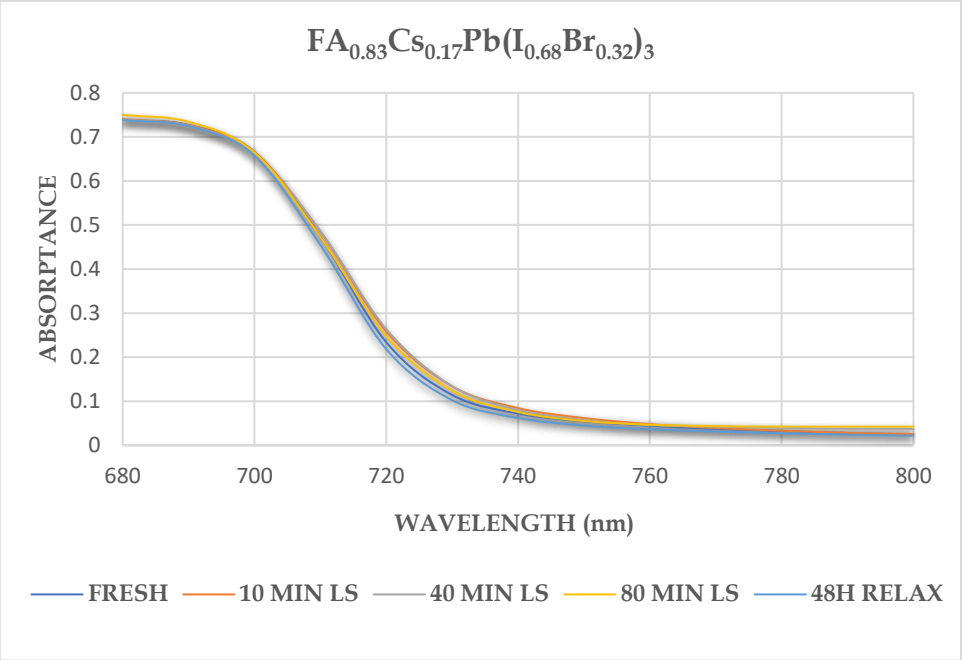

Figure 41 Calculated Spectral dependence of absorptance of perovskite on glass for composition $FA_{0.83}Cs_{0.17}Pb(I_{0.68}Br_{0.32})_3$

In figure 41 with $FA_{0.83}Cs_{0.17}Pb(I_{0.68}Br_{0.32})_3$ composition, the degradation of perovskite thin film can be hardly observed. The absorption edge shift after light-soaking for 80 min is negligible and the sharp absorption edge can be observed at all times including relaxation at λ= 700 nm. This composition showing only small changes compared to others can be termed as stable optical properties. When observed keenly, the absorption edge after 48hrs relaxation can be seen to return to original state. from its initial state can be clearly observed due to light soaking which tends to reduce the absorptance

of the cell and then measurement after 24H relaxation shows the absorptance edge shifted to the initial state.

Different compositions of perovskite cells have different bandgaps, where right composition can lead to higher efficiencies leading to better optoelectronic properties of the device [63]. We can observe different characteristics of absorptance dependent on the wavelength and it is interesting that, $FA_{0.83}Cs_{0.17}Pb(I_{0.68}Br_{0.32})_3$ showed

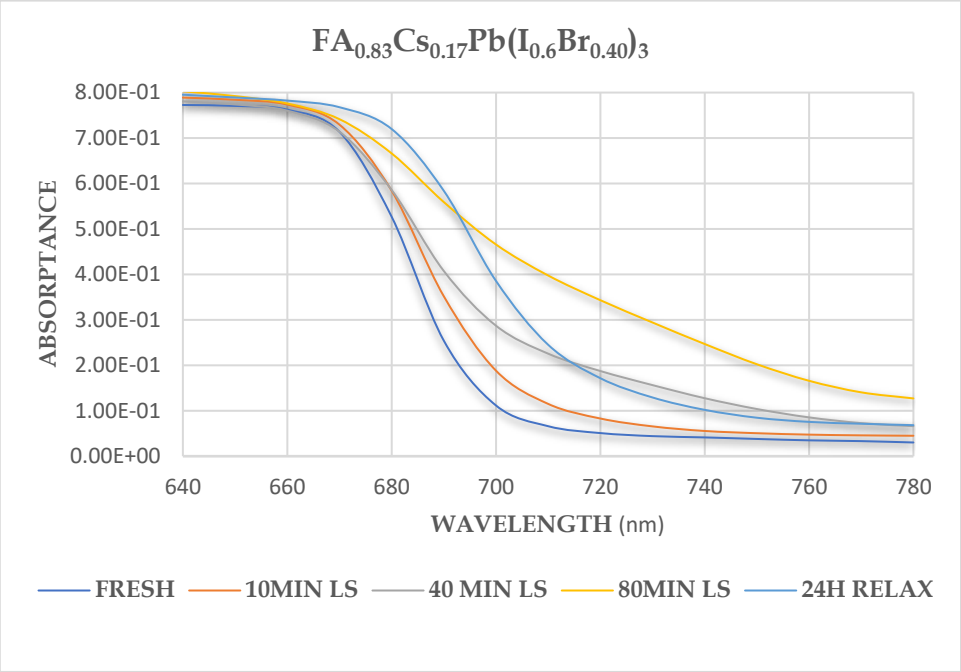

Figure 42 Calculated Spectral dependence of absorptance of perovskite on glass for composition $FA_{0.83}Cs_{0.17}Pb(I_{0.6}Br_{0.4})_3$

very small changes compared to other samples. The concentration of the absorber layers is therefore an important factor to be considered during the fabrication process. On the other hand, it can also mean, that the sample did not degrade as others after the light soaking it for 80 minutes. This is a thought-provoking observation and can be further studied into detail. Figure 42 with $FA_{0.83}Cs_{0.17}Pb(I_{0.6}Br_{0.4})_3$ brings out a different picture of the absorptance edges after light-soaking. The fresh sample showed sharp absorption edge at λ= 670 nm, after 80 min of light soaking the absorption edge is shifted from

λ= 670 nm to λ= 678 nm. Additionally, there is no sharp absorption edge observed but a smoother edge can be seen. The absorption edge is seemed to take a sharp form again at λ= 680 nm after 24hrs relaxation in the dark. Therefore, with this composition, the edge is shifted from λ= 670 nm to λ= 680 nm during illumination and relaxation cycle.

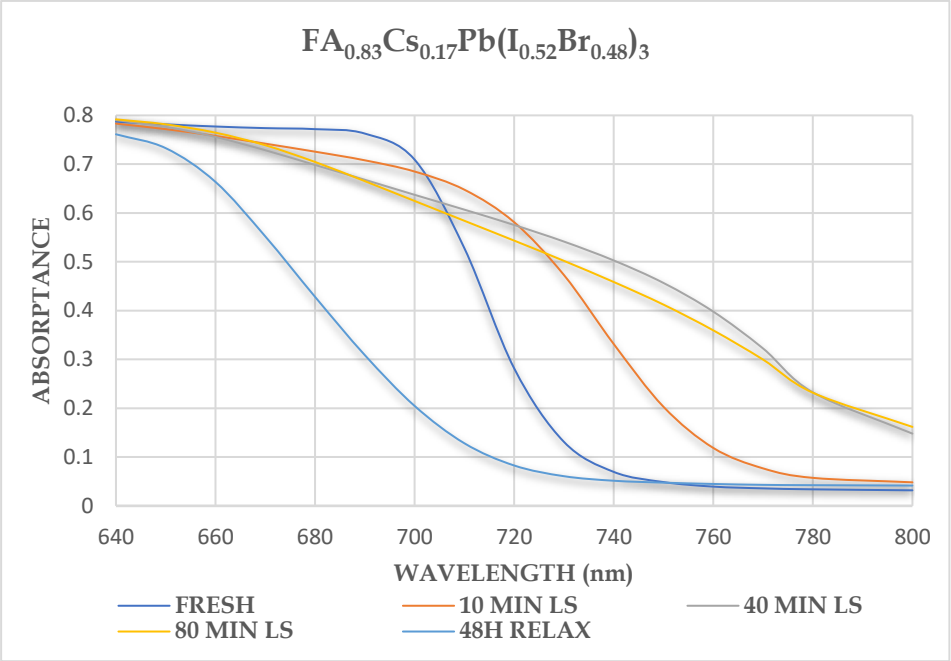

Figure 43 Calculated Spectral dependence of absorptance of perovskite on glass for composition $FA_{0.83}Cs_{0.17}Pb(I_{0.52}Br_{0.48})_3$

In figure 43 with $FA_{0.83}Cs_{0.17}Pb(I_{0.52}Br_{0.48})_3$ composition, there can be seen a lot of changes happening after the light soaking of the sample. These results could possibly occur due to change in Br content as it is increasing from the previous compositions of samples. There is a linear dependence observed between the bandgap and the Br content, as mentioned in [64]. These results can also be observed due to the fact that this sample was solely prepared by me and the instability of the sample can be observed due to it. Here, the fresh sample is showing a sharp absorption edge at λ= 700 nm and the characteristic after relaxation has reduced and absorption edge is

decreased to λ= 660 nm with a smoother absorption edge. The changes occurring with this composition are much more prominent compared to other samples.

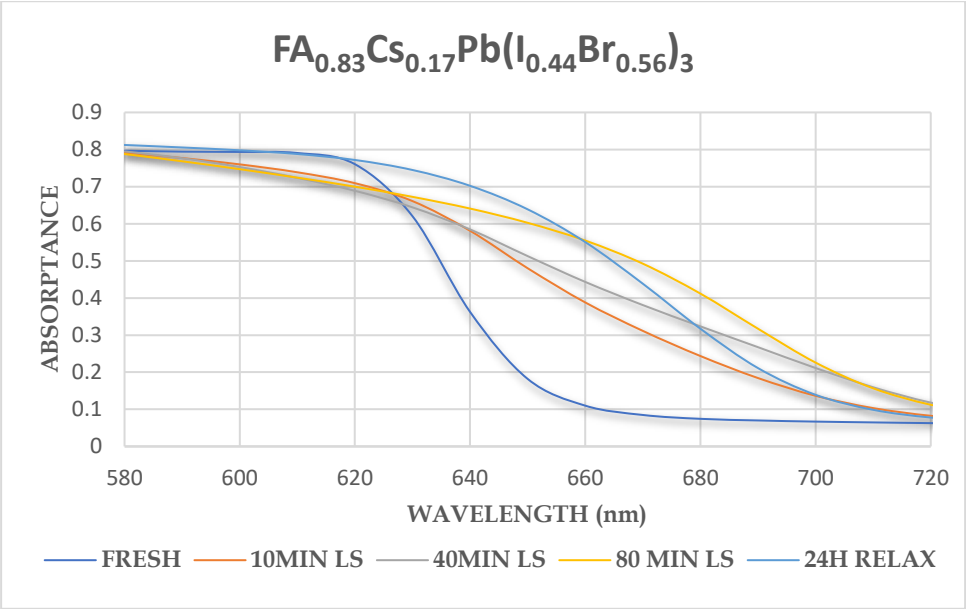

Figure 44 Calculated Spectral dependence of absorptance of perovskite on glass for composition $FA_{0.83}Cs_{0.17}Pb(I_{0.44}Br_{0.56})_3$

Figure 44 has $FA_{0.83}Cs_{0.17}Pb(I_{0.44}Br_{0.56})_3$ composition. The changes in this perovskite thin film sample shows a shift of absorption edge from λ= 620 nm to λ= 640 nm after relaxation of the sample for 24hrs, with not so sharp absorptance curve. This as mentioned earlier could be due to the increased Br content and change in morphology of the sample as it changes with increased Br content [64]. Many properties of this material are still unknown and can be studied in fair detail to understand the particular behaviour, characteristics and defects taking place in the device.

CONCLUSION

This thesis starts by discussing the need and advantages of renewable energy at current stage of evolution and focuses on the solar technology as a form of renewable energy. Fundamental concepts like materials and working of solar cell technology has been explained in brief. Working and some general terms in solar technology help in understanding the physics behind the technology. Chapter 4 helps in understanding the importance of bandgaps and tandem cells.

The chapters 5-11 completely focus on perovskite solar cell technology. Hypothetical Perovskite solar cell technology has the potential of achieving higher efficiencies and get closer to the theoretical SQ limit. The performance of the realistic device parameters show instability due to persistence of defects. To study the defects in mixed halide perovskite solar cells, here we have fabricated the cells with $FA_{0.83}Cs_{0.17}Pb(I_{0.6}Br_{0.4})_3$ composition. Single step spin coating method of fabrication is used for preparing the cells. The chapters also include in-depth method of preparation of perovskite solar cells. FTPS and I-V measurements to understand the phase segregation were performed on the similar composition. The behaviour and characteristics observed in both the measurements were also mentioned in the literature from many researchers. The samples on which the measurements were carried showed stable characteristics in the sub bandgap region. Therefore, the illumination was increased to 3 suns intensity. The results are included in Chapter 10, where we observed that these samples were more stable and to understand the small changes which happened, we focused on the fundamental mechanism of illumination and relaxation cycles. According to us the phase segregation can be due to larger grain size

and much better charge accumulation. Although not prominent, some changes are observed in the characteristics at sub-bandgap absorption and these changes could be due to presence of deep level defects as explained in Chapter 7. To figure out the exact type of deep level defect, more research and study is required. From the measured I-V curves, changes can be observed in the characteristics of the device during the illumination and relaxation regime. Decrease in V_{OC} in the relaxation cycle, could be due to presence of hysteresis or non-radiative recombination taking place in the cell. The samples also seemed to degrade due to the environmental effects. It is hard to pin point one reason for degradation of samples.

The last chapter focuses on varying the compositions of I-Br ratio to study the phase segregation in perovskite thin films. We deposited five different perovskite solutions with increasing Br content on glass substrate. This measurement was conducted using integrating sphere. From the calculated absorptance data, varying sharp absorption edges were observed for the five thin-films, the samples degraded during the light-soaking and tried to retain to its initial or close to initial state. This can be observed from the graphs included in Chapter 11. Out of all five samples $FA_{0.83}Cs_{0.17}Pb(I_{0.76}Br_{0.24})_3$ and $FA_{0.83}Cs_{0.17}Pb(I_{0.68}Br_{0.32})_3$, showed stable and better results which might be because of the compositions used while fabricating the thin films. The graphs show a drastic change in absorption edge beyond the Br content ($x > 0.32$). As mentioned in [64], the increasing Br content affect the performance of perovskite thin films, as there is a linear dependence between bandgap and increasing Br content. The crystal morphology also plays an important role in the device performance which also depends on the Br content. Thus, concluding that the composition of halides in perovskite solar cell

fabrication plays an important role, as they decide the efficiency and performance of the sample.

REFERENCES

[1] J. Holovsky, "Lecture 2 Problem of fossil fuels Solar energy form and availability on Earth Potential of its exploitation" Course- Solar System Applications, 2019.

[2] W. Rowley and A. Westwood, "The need for renewable energy," *Pet. Rev.*, vol. 57, no. 676, pp. 26–28, 2003.

[3] N. Guerra, M. Guevara, C. Palacios, and F. Crupi, "Operation and physics of photovoltaic solar cells: an overview," *I+D Tecnológico*, 2018, doi: 10.33412/idt.v14.2.2077.

[4] EPIA-_GP, "Solar photovoltaic electricity Solar generation 6 Solar photovoltaic electricity," 2011.

[5] J. Holovsky, "Lecture 3 Construction and technology of photovoltaic cells current cell technologies," Course- Solar System Applications 2020.

[6] L. Lin and N. M. Ravindra, "CIGS and perovskite solar cells – an overview," *Emerg. Mater. Res.*, vol. 9, no. 3, pp. 812–824, 2020, doi: 10.1680/jemmr.20.00124.

[7] R. B. Kodati and N. R. Puli, "a Review of Solar Cell Fundamentals and Technologies," *Adv. Sci. News*, no. September, 2020.

[8] N. G. Park, "Perovskite solar cells: An emerging photovoltaic technology," *Materials Today*. 2015, doi: 10.1016/j.mattod.2014.07.007.

[9] A. H. M. Smets, K. Jäger, O. Isabella, R. A. van Swaaij, and M. Zeman, *Solar Cell Parameters and Equivalent Circuit*. 2016.

[10] B. Ehrler, E. Alarcón-Lladó, S. W. Tabernig, T. Veeken, E. C. Garnett, and A. Polman, "Photovoltaics reaching for the shockley-queisser limit," *ACS Energy Lett.*, vol. 5, no. 9, pp. 3029–3033, Sep. 2020, doi: 10.1021/acsenergylett.0c01790.

[11] S. Gharibzadeh *et al.*, "Record Open-Circuit Voltage Wide-Bandgap Perovskite Solar Cells Utilizing 2D/3D Perovskite Heterostructure," *Adv. Energy Mater.*, 2019, doi: 10.1002/aenm.201803699.

[12] P. Kunwu Fu, P. Anita Wing Yi Ho-Baillie, P. Hemant Kumar Mulmudi, and P. Pham Thi Thu Trang, *Perovskite Solar Cells Technology and Practices*. .

[13] J. Holovský *et al.*, "Lead Halide Residue as a Source of Light-Induced Reversible Defects in Hybrid Perovskite Layers and Solar Cells," *ACS Energy Lett.*, 2019, doi: 10.1021/acsenergylett.9b02080.

[14] S. Mahesh *et al.*, "Revealing the origin of voltage loss in mixed-halide perovskite solar cells," *Energy Environ. Sci.*, 2020, doi: 10.1039/c9ee02162k.

[15] A. Peter Amalathas, L. Landová, B. Conrad, and J. Holovský, "Concentration-Dependent Impact of Alkali Li Metal Doped Mesoporous TiO2 Electron Transport Layer on the Performance of CH3NH3PbI3 Perovskite Solar Cells," *J. Phys. Chem. C*, 2019, doi: 10.1021/acs.jpcc.9b05355.

[16] Katja Vozel, "Seminar -1st year, 2nd cycle Solar Cells," *Nat. Energy*, 2014.

[17] M. Shyam, "Agro-residue-based renewable energy technologies for rural development," *Energy Sustain. Dev.*, vol. 6, no. 2, pp. 37–42, 2002, doi: 10.1016/S0973-0826(08)60311-7.

[18] B. C. Century, "Solar technology isn ' t new . Its history spans from the 7th Century B . C . to today . We started out concentrating the sun ' s heat with glass and mirrors to light fires . Today , we have everything from solar-powered buildings to solar- powered vehicl," *Glass*, 2000.

[19] T. W. Principle and S. Cell, "The Working Principle of a Solar Cell," *Sol. Energy*, 1921.

[20] "P/N Junctions and Band Gaps," *solarcentral.com*, 2014.

http://solarcellcentral.com/junction_page.html (accessed May 11, 2021).

[21] W. Shockley, W. Shockley, and H. J. Queisser, "The Shockley-Queisser limit," pp. 1–5, 1961.

[22] P. K. Nayak, S. Mahesh, H. J. Snaith, and D. Cahen, "Photovoltaic solar cell technologies: analysing the state of the art," *Nat. Rev. Mater.*, vol. 4, no. 4, pp. 269–285, 2019, doi: 10.1038/s41578-019-0097-0.

[23] J. Holovsk and L. Cost, "Lecture 10 Basic economical and ecological aspects," 2020.

[24] "Third-generation photovoltaics _ Elsevier Enhanced Reader.pdf." .

[25] S. Il Seok and T. F. Guo, "Halide perovskite materials and devices," *MRS Bull.*, vol. 45, no. 6, pp. 427–430, 2020, doi: 10.1557/mrs.2020.140.

[26] Fei Zhang and Kai Zhu, *Perovskite solar cells*. 2020.

[27] M. S. G. Hamed and G. T. Mola, "Mixed Halide Perovskite Solar Cells: Progress and Challenges," *Crit. Rev. Solid State Mater. Sci.*, vol. 45, no. 2, pp. 85–112, 2020, doi: 10.1080/10408436.2018.1549976.

[28] P. C. Reshmi Varma, "Low-dimensional perovskites," in *Perovskite Photovoltaics: Basic to Advanced Concepts and Implementation*, 2018.

[29] C. N. R. Rao, "Perovskites," in *Encyclopedia of Physical Science and Technology*, 2003.

[30] S. T. Ha, R. Su, J. Xing, Q. Zhang, and Q. Xiong, "Metal halide perovskite nanomaterials: synthesis and applications," *Chem. Sci.*, vol. 8, no. 4, pp. 2522–2536, 2017, doi: 10.1039/c6sc04474c.

[31] I. Hussain, H. P. Tran, J. Jaksik, J. Moore, N. Islam, and M. J. Uddin, "Functional materials, device architecture, and flexibility of perovskite solar cell," *Emergent Mater.*, vol. 1, no. 3–4, pp. 133–154, 2018, doi: 10.1007/s42247-018-0013-1.

[32] S. Pitchaiya *et al.*, "A review on the classification of organic/inorganic/carbonaceous hole transporting materials for perovskite solar cell application," *Arab. J. Chem.*, vol. 13, no. 1, pp. 2526–2557, 2020, doi: 10.1016/j.arabjc.2018.06.006.

[33] P. Roy, N. Kumar Sinha, S. Tiwari, and A. Khare, "A review on perovskite solar cells: Evolution of architecture, fabrication techniques, commercialization issues and status," *Sol. Energy*, vol. 198, no. January, pp. 665–688, 2020, doi: 10.1016/j.solener.2020.01.080.

[34] Ç. Şahin, H. Diker, D. Sygkridou, C. Varlikli, and E. Stathatos, "Enhancing the efficiency of mixed halide mesoporous perovskite solar cells by introducing amine modified graphene oxide buffer layer," *Renew. Energy*, vol. 146, pp. 1659–1666, 2020, doi: 10.1016/j.renene.2019.07.162.

[35] F. Ullah, H. Chen, and C. Z. Li, "Organic functional materials based buffer layers for efficient perovskite solar cells," *Chinese Chem. Lett.*, vol. 28, no. 3, pp. 503–511, 2017, doi: 10.1016/j.cclet.2016.11.009.

[36] D. Yang, R. Yang, S. Priya, and S. (Frank) Liu, "Recent Advances in Flexible Perovskite Solar Cells: Fabrication and Applications," *Angew. Chemie - Int. Ed.*, vol. 58, no. 14, pp. 4466–4483, 2019, doi: 10.1002/anie.201809781.

[37] K. Mahmood, S. Sarwar, and M. T. Mehran, "Current status of electron transport layers in perovskite solar cells: materials and properties," *RSC Adv.*, vol. 7, no. 28, pp. 17044–17062, 2017, doi: 10.1039/c7ra00002b.

[38] "Bischak et al. - 2017 - Origin of Reversible Photoinduced Phase Separation.pdf." .

[39] M. I. Ahmed, A. Habib, and S. S. Javaid, "Perovskite Solar Cells: Potentials, Challenges, and Opportunities," *Int. J. Photoenergy*, vol. 2015, no. October, 2015, doi: 10.1155/2015/592308.

[40] Y. Yao, X. Zou, J. Cheng, T. Ling, C. Chang, and D. Chen, "Impact of

K+ doping on modulating majority charge carrier type and quality of perovskite thin films by two-step solution method for solar cells," *Coatings*, vol. 9, no. 10, 2019, doi: 10.3390/coatings9100647.

[41] S. M. I. Hossain, "Performance and stability of perovskite solar cells," p. 256, 2018.

[42] S. G. Motti *et al.*, "Defect Activity in Lead Halide Perovskites," *Adv. Mater.*, vol. 31, no. 47, pp. 1–11, 2019, doi: 10.1002/adma.201901183.

[43] A. Maiti, S. Chatterjee, L. Peedikakkandy, and A. J. Pal, "Defects and Their Passivation in Hybrid Halide Perovskites toward Solar Cell Applications," *Sol. RRL*, vol. 4, no. 12, 2020, doi: 10.1002/solr.202000505.

[44] A. J. Knight and L. M. Herz, "Preventing phase segregation in mixed-halide perovskites: A perspective," *Energy and Environmental Science*, vol. 13, no. 7. Royal Society of Chemistry, pp. 2024–2046, Jul. 01, 2020, doi: 10.1039/d0ee00788a.

[45] A. J. Knight *et al.*, "Electronic Traps and Phase Segregation in Lead Mixed-Halide Perovskite," 2018, doi: 10.1021/acsenergylett.8b02002.

[46] M. C. Brennan, S. Draguta, P. V Kamat, and M. Kuno, "Light-Induced Anion Phase Segregation in Mixed Halide Perovskites," *Cite This ACS Energy Lett*, vol. 3, pp. 204–213, 2018, doi: 10.1021/acsenergylett.7b01151.

[47] M. C. Brennan, S. Draguta, P. V. Kamat, and M. Kuno, "Light-Induced Anion Phase Segregation in Mixed Halide Perovskites," *ACS Energy Letters*, vol. 3, no. 1. pp. 204–213, 2018, doi: 10.1021/acsenergylett.7b01151.

[48] A. J. Knight and L. M. Herz, "Preventing phase segregation in mixed-halide perovskites: A perspective," *Energy Environ. Sci.*, vol. 13, no. 7, pp. 2024–2046, 2020, doi: 10.1039/d0ee00788a.

[49] K. Vandewal *et al.*, "Fourier-Transform Photocurrent Spectroscopy for

a fast and highly sensitive spectral characterization of organic and hybrid solar cells," *Thin Solid Films*, vol. 516, no. 20, pp. 7135–7138, 2008, doi: 10.1016/j.tsf.2007.12.056.

[50] J. Holovský *et al.*, "Towards quantitative interpretation of fourier-transform photocurrent spectroscopy on thin-film solar cells," *Coatings*, vol. 10, no. 9, pp. 1–9, 2020, doi: 10.3390/coatings10090820.

[51] R. A. Sinton and A. Cuevas, "Contactless determination of current-voltage characteristics and minority-carrier lifetimes in semiconductors from quasi-steady-state photoconductance data," *Appl. Phys. Lett.*, vol. 69, no. 17, pp. 2510–2512, Oct. 1996, doi: 10.1063/1.117723.

[52] "Short-Circuit Current | PVEducation." https://www.pveducation.org/pvcdrom/solar-cell-operation/short-circuit-current (accessed May 18, 2021).

[53] "Fill Factor | PVEducation." https://www.pveducation.org/pvcdrom/solar-cell-operation/fill-factor (accessed May 11, 2021).

[54] D. Guo, Z. Andaji Garmaroudi, M. Abdi-Jalebi, S. D. Stranks, and T. J. Savenije, "Reversible Removal of Intermixed Shallow States by Light Soaking in Multication Mixed Halide Perovskite Films," *ACS Energy Lett.*, vol. 4, no. 10, pp. 2360–2367, 2019, doi: 10.1021/acsenergylett.9b01726.

[55] S. G. Motti *et al.*, "Controlling competing photochemical reactions stabilizes perovskite solar cells," *Nat. Photonics*, vol. 13, no. 8, pp. 532–539, 2019, doi: 10.1038/s41566-019-0435-1.

[56] T. Duong *et al.*, "Light and Electrically Induced Phase Segregation and Its Impact on the Stability of Quadruple Cation High Bandgap Perovskite Solar Cells," *ACS Appl. Mater. Interfaces*, vol. 9, no. 32, pp. 26859–26866, 2017, doi: 10.1021/acsami.7b06816.

[57] D. T. Limmer and N. S. Ginsberg, "Photoinduced phase separation in

the lead halides is a polaronic effect," *J. Chem. Phys.*, vol. 152, no. 23, 2020, doi: 10.1063/1.5144291.

[58] X. Tang *et al.*, "Local Observation of Phase Segregation in Mixed-Halide Perovskite," *Nano Lett.*, vol. 18, no. 3, pp. 2172–2178, 2018, doi: 10.1021/acs.nanolett.8b00505.

[59] M. Abdi-Jalebi *et al.*, "Maximizing and stabilizing luminescence from halide perovskites with potassium passivation," *Nature*, vol. 555, no. 7697, pp. 497–501, 2018, doi: 10.1038/nature25989.

[60] "light indiced phase segregation.pdf." .

[61] O. N. The, *Effect of light*, no. 2. 1957.

[62] "reversible photo induced trap formation in mixed halide perovskite.pdf." .

[63] M. Anaya, *Optical design of perovskite materials and solar cells*. 2018.

[64] D. Cui *et al.*, "Color-Tuned Perovskite Films Prepared for Efficient Solar Cell Applications," *J. Phys. Chem. C*, vol. 120, no. 1, pp. 42–47, 2016, doi: 10.1021/acs.jpcc.5b09393.